Hierarchical assembly of the eggshell and permeability barrier in *C. elegans*

Sara K. Olson,[1] Garrett Greenan,[2] Arshad Desai,[1] Thomas Müller-Reichert,[3] and Karen Oegema[1]

[1]Ludwig Institute for Cancer Research, Department of Cellular and Molecular Medicine, University of California, San Diego, La Jolla, CA 92093
[2]Max Planck Institute of Molecular Cell Biology and Genetics, 01307 Dresden, Germany
[3]Medical Theoretical Center, Dresden University of Technology, 01307 Dresden, Germany

In metazoans, fertilization triggers the assembly of an extracellular coat that constitutes the interface between the embryo and its environment. In nematodes, this coat is the eggshell, which provides mechanical rigidity, prevents polyspermy, and is impermeable to small molecules. Using immunoelectron microscopy, we found that the *Caenorhabditis elegans* eggshell was composed of an outer vitelline layer, a middle chitin layer, and an inner layer containing chondroitin proteoglycans. The switch between the chitin and proteoglycan layers was achieved by internalization of chitin synthase coincident with exocytosis of proteoglycan-containing cortical granules. Inner layer assembly did not make the zygote impermeable as previously proposed. Instead, correlative light and electron microscopy demonstrated that the permeability barrier was a distinct envelope that formed in a separate step that required fatty acid synthesis, the sugar-modifying enzyme PERM-1, and the acyl chain transfer enzyme DGTR-1. These findings delineate the hierarchy of eggshell assembly and define key molecular mechanisms at each step.

Introduction

Oocytes from all animal species have a special coat of ECM that has different names depending on the species (Foor, 1967; Wharton, 1980; Wong and Wessel, 2006): the zona pellucida in mammals, the chorion in fish, the vitelline envelope in amphibians, mollusks, and crustaceans, and the vitelline layer in echinoderms and nematodes. The oocyte ECM coat mediates sperm binding and is modified after fertilization, often dramatically, to prevent polyspermy and to generate a covering to protect the zygote. The processes that modify the ECM coat vary between species; however, there are many common themes (Wong and Wessel, 2006). Postfertilization coats are assembled from material stored in the oocyte, although supporting cells can also modify the coat from the outside. Coat assembly usually involves exocytosis of specialized secretory vesicles that contain structural proteins and ECM-modifying enzymes, called cortical granules. Cortical granule exocytosis promotes separation of the vitelline layer from the embryo surface, generating an intervening "perivitelline" space.

Correspondence to Karen Oegema: koegema@ucsd.edu

S.K. Olson's present address is Dept. of Biology, Pomona College, Claremont, CA 91711.

Abbreviations used in this paper: CAV-1, caveolin-1; CCD, charge-coupled device; CDP, cytidine diphosphate; CPG, chondroitin proteoglycan; DIC, differential interference contrast; dsRNA, double-stranded RNA; GlcNAc, *N*-acetylglucosamine.

The nematode postfertilization ECM coat is a trilaminar eggshell that has been proposed to be comprised of an outer vitelline layer, a middle chitin layer, and an inner lipid layer that acts as a permeability barrier that prevents the passage of small molecules (Wharton 1980; Mansfield et al., 1992; Rappleye et al., 1999; Bembenek et al., 2007; Benenati et al., 2009). The outer vitelline layer stains with wheat germ agglutinin (Johnston et al., 2006), suggesting that it contains glycoproteins with *N*-acetylglucosamine (GlcNAc) and/or *N*-acetylgalactosamine carbohydrate modifications (Natsuka et al., 2005), but no protein components have been identified. Fertilization is thought to activate chitin synthase (CHS-1), a multipass transmembrane protein that polymerizes cytosolic UDP-GlcNAc into the secreted β1,4-linked GlcNAc homopolymer, chitin (Zhang et al., 2005). Chitin is thought to be deposited under the vitelline layer immediately after fertilization (Maruyama et al., 2007), in a step that is essential to prevent polyspermy (Johnston et al., 2010). The next step of eggshell assembly occurs ∼15 min after fertilization at anaphase of meiosis I, concurrent with a wave of cortical granule exocytosis (Bembenek et al., 2007). Exocytosed

The Rockefeller University Press $30.00
J. Cell Biol. Vol. 198 No. 4 731–748
www.jcb.org/cgi/doi/10.1083/jcb.201206008

cortical granule cargo is proposed to build the inner eggshell layer and generate the permeability barrier. Cortical granules stain with an antibody against chondroitin (Sato et al., 2008), suggesting that the redundant chondroitin proteoglycans (CPGs) CPG-1 and CPG-2, which are required for eggshell impermeability, may be important cargoes (Johnston et al., 2006; Olson et al., 2006; Bembenek et al., 2007). Fatty acid biosynthesis and modification enzymes have also been reported to be essential for eggshell impermeability and assembly of the inner eggshell layer (Tagawa et al., 2001; Rappleye et al., 2003; Benenati et al., 2009; Carvalho et al., 2011).

Using immunoelectron microscopy, we show that the *Caenorhabditis elegans* eggshell is composed of an outer vitelline layer, a middle chitin layer, and an inner layer containing CPG-1 and CPG-2. A precise switch between assembly of the chitin and CPG layers occurs when chitin synthase is internalized from the cell surface concurrent with exocytosis of cortical granules carrying CPG-1/2 at anaphase of meiosis I. Surprisingly, cortical granule exocytosis and completion of the trilaminar shell did not confer impermeability to small molecules as previously proposed. Correlative light and electron microscopy revealed that the permeability barrier is a distinct envelope between the trilaminar shell and the embryo plasma membrane that forms in a separate step. Permeability barrier formation requires passage through anaphase of meiosis II, fatty acid biosynthesis, the sugar-modifying enzyme PERM-1, and the acyl chain transfer enzyme DGTR-1. These molecular requirements suggest that an ascaroside glycolipid may be an essential constituent of the permeability barrier. These findings define the hierarchical assembly of the nematode eggshell after fertilization, delineate the event of permeability barrier formation, and establish the key molecular mechanisms operating at each step.

Results

Chitin and the CPG-1/2 localize to the middle and inner layers of the trilaminar eggshell, respectively

In electron micrographs, the *C. elegans* eggshell appears trilaminar, consisting of a thin, electron-dense outer vitelline layer and thicker middle and inner layers (Fig. 1 A; Rappleye et al., 1999). Chitin synthesis is thought to begin immediately after fertilization to form the middle layer. Cortical granules are exocytosed beginning ∼15 min after fertilization (Bembenek et al., 2007). Candidate cortical granule cargoes for incorporation into the eggshell include the functionally redundant CPGs CPG-1 and CPG-2 (Olson et al., 2006; Bembenek et al., 2007; Sato et al., 2008). CPG-1 and CPG-2 contain chitin-binding domains (Fig. 1 C), suggesting that they either form a mixed matrix with chitin within one eggshell layer or are incorporated into a separate layer adjacent to one that contains chitin. Localization of CPG-1/2 and chitin, which had not previously been examined at the ultrastructural level, by immunoelectron microscopy of high-pressure frozen embryos revealed that chitin was confined almost exclusively to the middle eggshell layer (91.3%, $n = 543$ gold particles and 4 embryos; Fig. 1 B). CPG-1 and CPG-2 were localized using two antibodies: one that recognizes both proteins and one that specifically recognizes CPG-2 (Fig. S1 A). The localization of both CPG antibodies was restricted to the inner eggshell layer (99% for α–CPG-1/2, $n = 1{,}412$ gold particles and 4 embryos; 96% for α–CPG-2, $n = 311$ gold particles and 4 embryos; Fig. 1 C). We conclude that instead of forming a mixed matrix, chitin is deposited in the middle layer, whereas the CPG-1/2 proteoglycans are incorporated into the innermost layer of the trilaminar shell.

Chitin synthase is internalized concurrent with cortical granule exocytosis, facilitating the deposition of chitin and CPG-1/2 in sequential layers

Cortical granules, which can be followed using the marker caveolin-1 (CAV-1; Sato et al., 2006; Bembenek et al., 2007), stain with an antibody to chondroitin (Sato et al., 2008). To determine whether this is because the CPG-1/2 proteoglycans are cortical granule cargo, we imaged transgenic strains expressing mCherry fusions with CPG-1 or CPG-2 (Fig. 2, A and B). Before anaphase of meiosis I, both CPG probes localized within cytoplasmic cortical granules marked with GFP::CAV-1 (Fig. S2, A and B). After cortical granule exocytosis at anaphase I, mCherry::CPG-1 localized to the eggshell (Fig. 2 A). mCherry::CPG-1 fluorescence did not recover after photobleaching ($n = 10$), indicating that CPG-1 is stably incorporated into the eggshell (Fig. S2, C and E; and Video 1). In contrast to mCherry::CPG-1, the majority of mCherry::CPG-2 remained in the perivitelline space between the eggshell and embryo after its release from cortical granules (Fig. 2 B). mCherry::CPG-2 fluorescence rapidly recovered ($t_{1/2} = 8 \pm 1.8$ s SD, $n = 10$) after photobleaching, indicating that it can freely diffuse within the perivitelline space (Fig. S2, D and F; and Video 2). Failure to preserve this freely diffusible CPG-2 likely explains why it is not observed in fixed analysis (Figs. 1 C and S1 C). Consistent with this idea, mCherry::CPG-2 and endogenous CPG-2 are similarly confined to the eggshell in fixed embryos (Fig. S1 C). CPG-2 has 34 consensus sites for chondroitin attachment compared with five for CPG-1 (Fig. 1 C; Olson et al., 2006), suggesting that on average CPG-2 may be more glycosylated than CPG-1 and thus more likely to remain soluble in the perivitelline space. Consistent with this explanation, mCherry::CPG-2 localized to the eggshell, rather than the perivitelline space, in embryos depleted of SQV-5, the enzyme responsible for elongating chondroitin chains (Fig. 2 B). This analysis identifies the cortical granule components CPG-1 and CPG-2 as the first described components of the inner eggshell layer, which we will subsequently refer to as the CPG layer, and suggests that CPG-2 localizes to both the CPG layer and to the perivitelline space.

To understand how chitin and CPG-1/2 are restricted to the middle and inner layers, respectively, we imaged embryos coexpressing mCherry::CPG-2 and a GFP fusion with the chitin synthase CHS-1 (Maruyama et al., 2007), a multipass transmembrane protein that secretes chitin into the extracellular space. Release of mCherry::CPG-2 at anaphase of meiosis I (Fig. 2, C and D; and Video 3) was temporally coupled to the previously described internalization of GFP::CHS-1 (Maruyama et al., 2007;

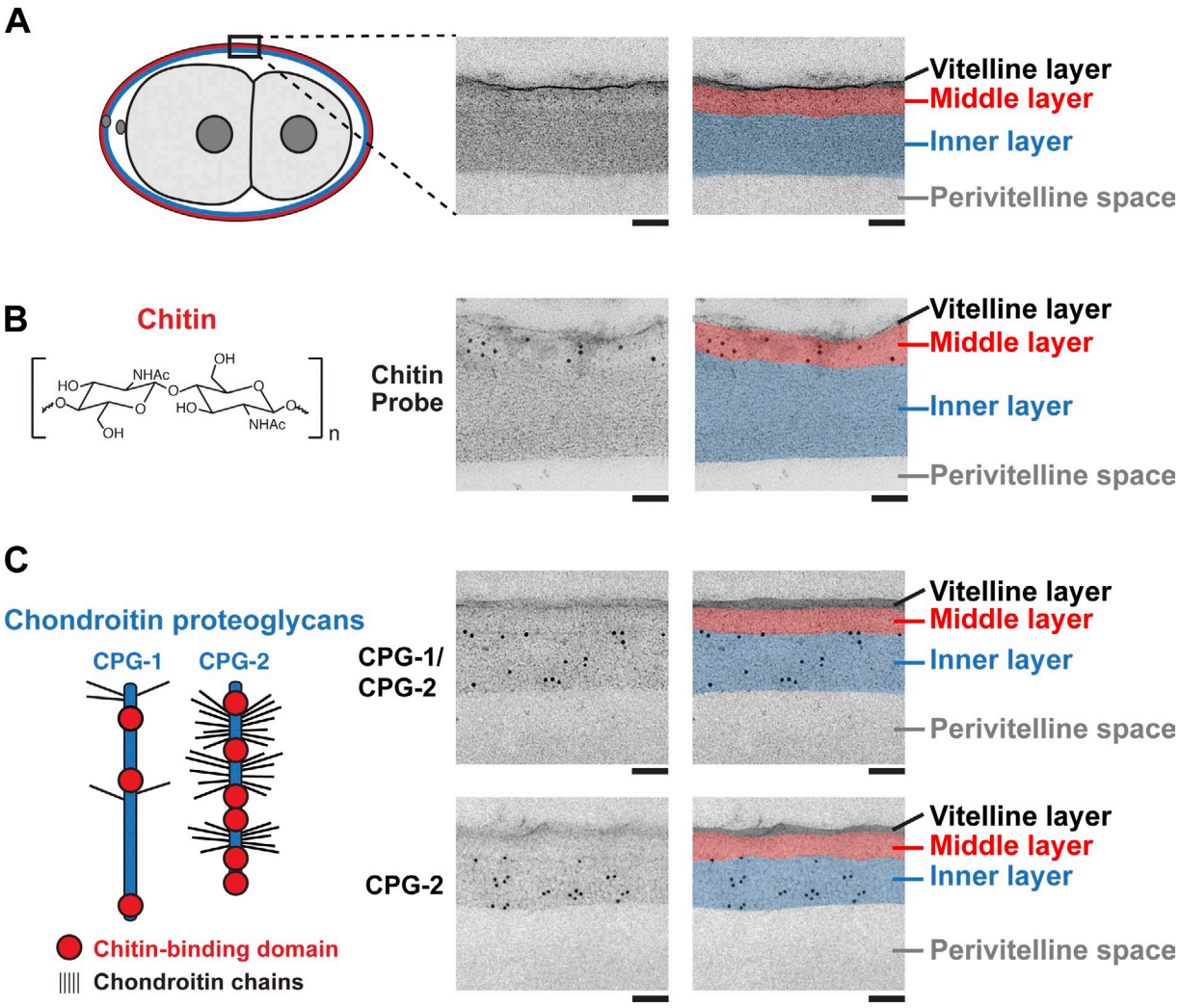

Figure 1. **Chitin and the CPG-1/2 localize to the middle and inner layers of the trilaminar eggshell, respectively.** (middle) Transmission electron micrographs of the eggshell in high-pressure frozen embryos. (right) Pseudocolored micrographs illustrate the location of the outer (black), middle, and inner eggshell layers. Beneath the inner layer is the perivitelline space between the eggshell and embryo plasma membrane. (A, left) A schematic is provided for orientation, with the black box highlighting the imaged region. (B) Chitin is composed of repeating units of β1,4-linked *N*-acetylglucosamine. Image is an electron micrograph of an eggshell after immunogold labeling (10-nm gold beads) with a chitin-binding probe. (C) CPG-1 and CPG-2 are secreted CPGs composed of a protein core (blue) with covalently linked chondroitin side chains (thin black lines are putative chondroitin attachment sites based on sequence consensus; Olson et al., 2006) and chitin-binding domains. Images are electron micrographs of eggshells after immunogold labeling (10-nm beads) using antibodies recognizing both CPG-1 and CPG-2 (top) or specifically CPG-2 (bottom). Bars, 100 nm.

Stitzel et al., 2007). CPG-1/2 depletion delayed GFP::CHS-1 internalization (Fig. 2 E) and led to formation of a chitin layer that is ∼1.6-fold thicker than controls (Fig. 3 C). We conclude that temporal coupling of chitin synthase internalization to cortical granule release may contribute to establishing the sharp boundary between the middle chitin and inner CPG eggshell layers.

Formation of the inner CPG layer requires prior deposition of the chitin layer

As anticipated based on their sequential deposition, chitin deposition did not require CPG-1/2 (Fig. 3 A). In the converse experiment, mCherry::CPG-1 was not deposited in the eggshell when chitin synthesis was inhibited (Fig. 3 A). This result suggests that the chitin layer scaffolds assembly of the CPG layer, potentially through interactions between chitin and the chitin-binding domains of CPG-1/2. Consistent with chitin layer assembly being upstream of CPG-1/2 deposition, inhibition of CPG-1/2 resulted in a less severe phenotype than inhibition of chitin synthase. Even when dissected into osmotic support medium, *cpg-1/2(RNAi)* embryos were swollen within the eggshell, with their plasma membranes adhered to the inside of the shell (Fig. 3 B). *cpg-1/2(RNAi)* embryos had a scalloped appearance because the plasma membrane detached from the shell in small regions to generate pockets of perivitelline space (Video 4). When chitin synthesis was inhibited through CHS-1 depletion, scallops were also observed. In addition, the eggshells frequently ruptured, causing the embryo to extrude out of the shell (Fig. 3 B and see Fig. 6 C and Video 5). We conclude that the chitin and CPG layers assemble in a hierarchical fashion. Chitin layer deposition is required for the subsequent assembly of the CPG layer and for the mechanical integrity of the eggshell.

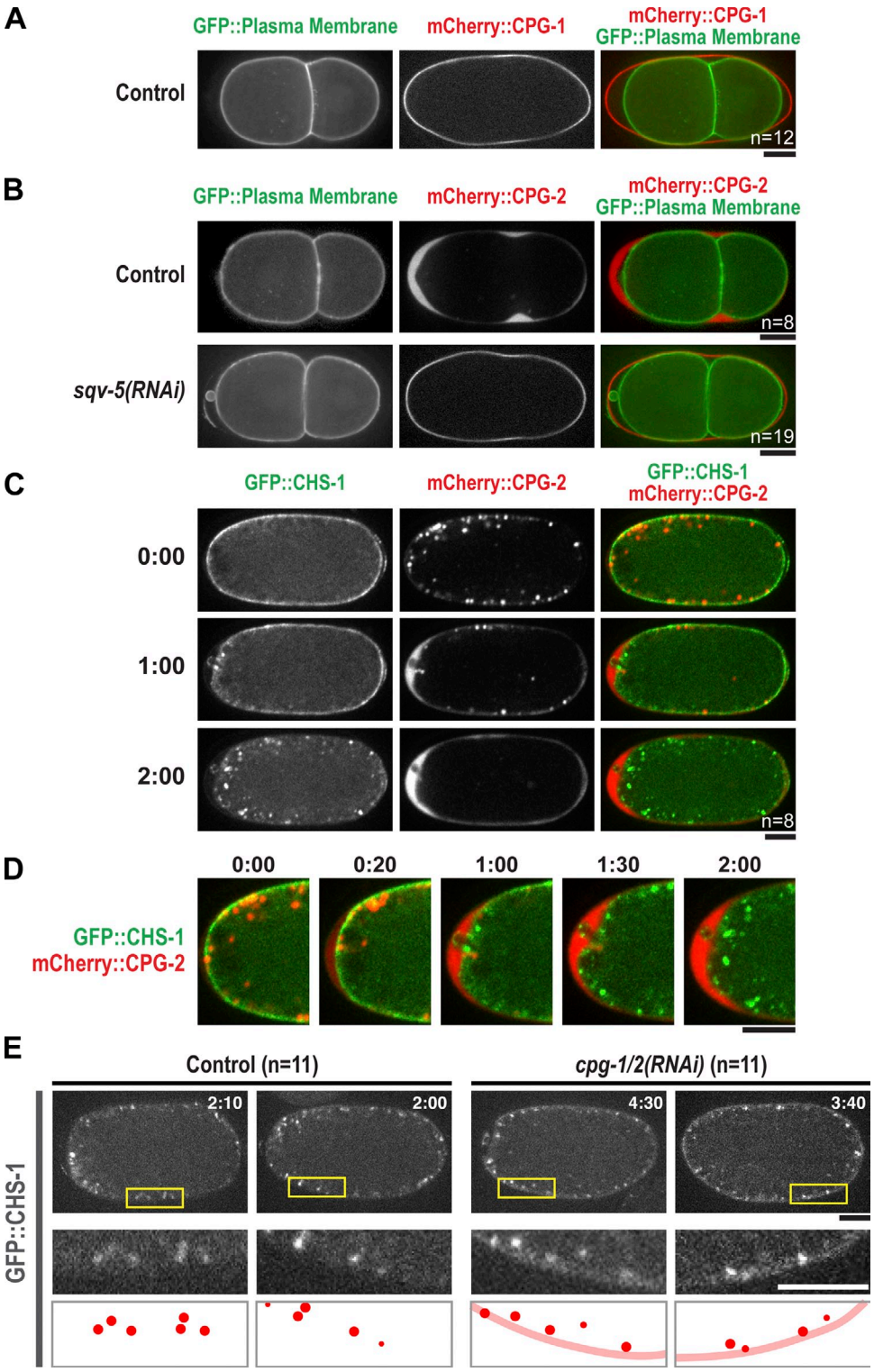

Figure 2. **Chitin synthase is internalized concurrent with cortical granule exocytosis, facilitating the deposition of chitin and CPG-1/2 in sequential layers.** (A) Confocal images of a two-cell stage embryo expressing a GFP-labeled plasma membrane probe (left) and mCherry::CPG-1 (middle). (B) Confocal images of two-cell stage control (top) and *sqv-5(RNAi)* (bottom) embryos expressing a GFP-labeled plasma membrane probe (left) and mCherry::CPG-2 (middle). (C) Time-lapse confocal images of a one-cell stage embryo expressing GFP::CHS-1 (left) and mCherry::CPG-2 (middle). Times are minutes and seconds after anaphase I. Embryo anterior is on the left. (D) Higher magnification view of the anterior of embryo in C. (E) Confocal images of two control (left) and two *cpg-1/2(RNAi)* (right) embryos expressing GFP::CHS-1. Times are minutes and seconds past anaphase I, when CHS-1 normally starts to internalize from the plasma membrane into subcortical puncta. Boxed regions are magnified below. Schematics highlight GFP::CHS-1 localization. By 2 min after anaphase I, the majority of GFP::CHS-1 in control embryos has been internalized into puncta (red spheres). In *cpg-1/2(RNAi)* embryos at a later time point, ∼4 min after anaphase I, some GFP::CHS-1 have internalized into puncta, but some also remain associated with the plasma membrane (red line). Bars, 10 µm. *n* = number of imaged embryos.

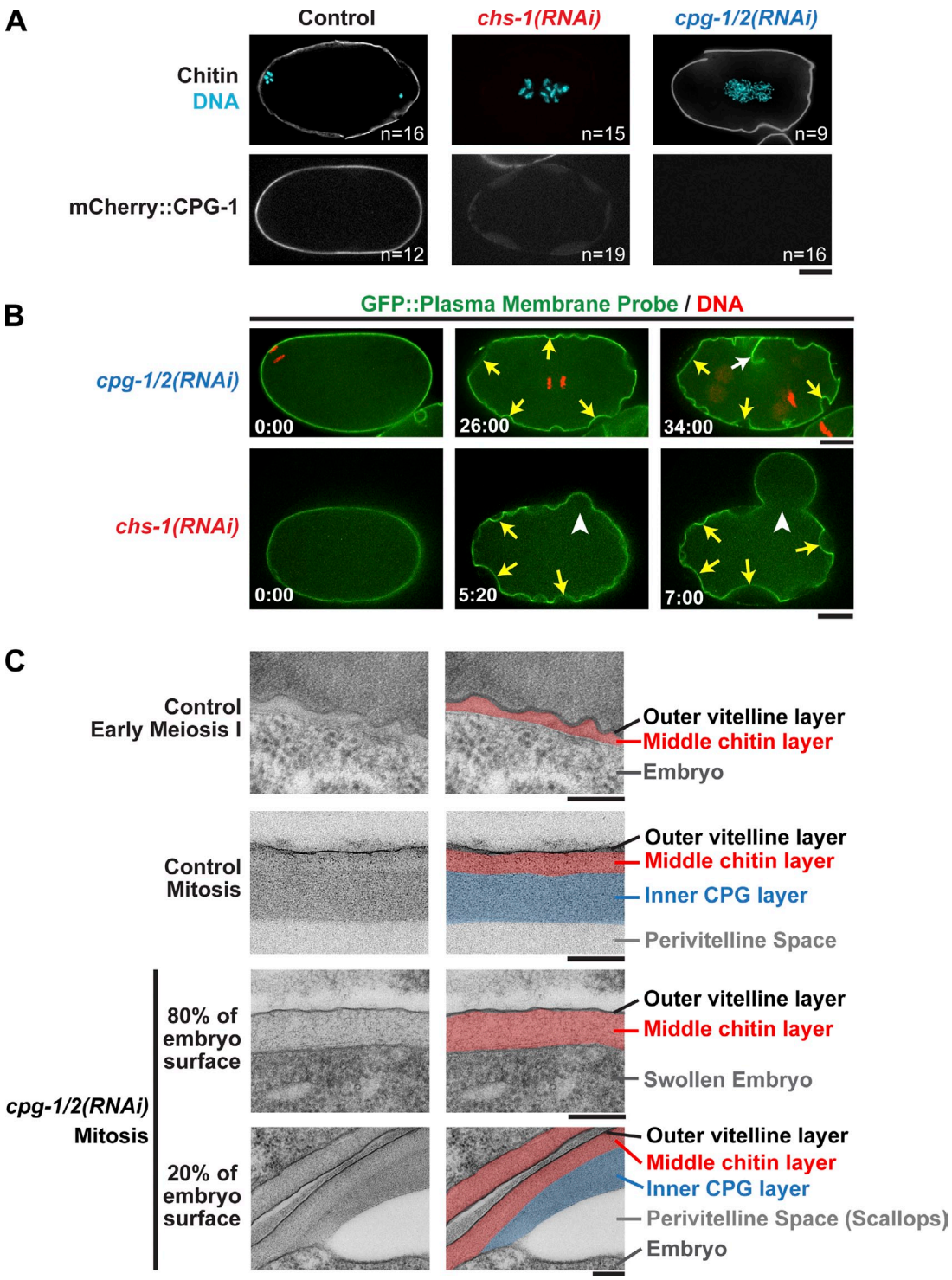

Figure 3. **Formation of the inner CPG layer requires prior deposition of the chitin layer.** (A, top) Immunofluorescence images of embryos stained with a chitin-binding probe (white) and for DNA. (bottom) Confocal images of embryos expressing mCherry::CPG-1. (B) Confocal images of *cpg-1/2(RNAi)* (top; *n* = 23) and *chs-1(RNAi)* (bottom; *n* = 26) embryos expressing a GFP-labeled plasma membrane probe and mCherry::histone H2B. Locations where the plasma membrane is able to separate from the eggshell (scallops; yellow arrows), a failed attempt at cytokinesis (white arrow) and a point where the eggshell lost integrity (rupture; white arrowheads) are marked. Times are minutes and seconds after the first frame. (C) Transmission electron micrographs of high-pressure frozen embryos. (right) Pseudocolored micrographs illustrate the location of the vitelline, chitin, and CPG layers. The mitotic control image is reproduced from Fig. 1 A for comparison. Bars: (A and B) 10 µm; (C) 200 nm. *n* = number of imaged embryos.

CPG-1/2 are required for the formation of the inner CPG layer

In electron micrographs of early embryos, fixed by high-pressure freezing at time points between fertilization and anaphase of meiosis I, a chitin layer was present between the vitelline layer and the embryo plasma membrane, but there was no CPG layer or perivitelline space. In later mitotically dividing embryos, the trilaminar eggshell was complete, and the perivitelline space

was present (Fig. 3 C). In mitotic *cpg-1/2(RNAi)* embryos, the majority (~80%) of the embryo plasma membrane was immediately juxtaposed to the chitin layer as in control embryos fixed before anaphase I. The chitin layer was thicker than in controls (131 ± 25 nm SD in *cpg-1/2(RNAi)*, $n = 56$ fields, and $n = 8$ embryos; vs. 80 ± 16 nm in wild type, $n = 30$ fields, and $n = 6$ embryos), and there was no intervening inner layer or perivitelline space. However, within the scallops, which covered ~20% (20.5 ± 13% SD, $n = 6$ embryos) of the embryo surface, an inner layer was present (Fig. 3 C). We suspect that this partial inner layer is caused by residual CPG-1/2. We conclude that CPG-1/2 are required for formation of the CPG layer and that the CPG layer is in turn required to detach the plasma membrane from the chitin layer and open up the perivitelline space.

Formation of a permeability barrier requires passage through anaphase of meiosis II

Nematode eggshells contain a permeability barrier virtually unrivaled in the animal kingdom that limits the diffusion of water and small molecular weight solutes, while still allowing for gas exchange (Christenson, 1950; Fairbairn, 1957; Anya, 1976). The inner layer of the trilaminar shell has been proposed to be the permeability barrier. Consistent with this idea, inhibition of chitin synthase or CPG-1/2 results in permeable embryos that take up FM4-64 dye (Johnston et al., 2006). FM4-64 is excluded by intact eggshells but passes through permeable eggshells and fluoresces upon binding to the plasma membrane (Fig. 4 A). To determine when the permeability barrier forms, we monitored the ability of embryos at different developmental stages to take up FM4-64 dye. Because the inner CPG layer is deposited during anaphase of meiosis I, we anticipated that the permeability barrier would be formed at this time. Contrary to this expectation, embryos remained permeable for ~14 min past anaphase of meiosis I and only became impermeable at anaphase of meiosis II (Fig. 4 B). These data suggested two possibilities: (1) cortical granule cargoes form the permeability barrier, but the barrier takes ~14 min to mature after exocytosis, or (2) formation of the permeability barrier is a distinct event that requires passage through anaphase of meiosis II. To distinguish between these possibilities, we artificially extended the time interval between anaphase of meiosis I and II. Embryos depleted of the CUL-2 E3 ubiquitin ligase progress normally through anaphase of meiosis I and release cortical granule cargo (Fig. 4 C) but then enter a prolonged metaphase II, which extends the time interval between anaphase of meiosis I and II from 14 min to ~50 min (Liu et al., 2004; Sonneville and Gönczy, 2004). CUL-2 depletion led to a delay in permeability barrier formation comparable with the delay induced in onset of anaphase of meiosis II (Fig. 4 D). We conclude that permeability barrier formation represents a previously unappreciated distinct step that requires passage through anaphase of meiosis II.

The permeability barrier is a distinct envelope that assembles between the embryo plasma membrane and trilaminar eggshell

The fact that the permeability layer forms during anaphase II, whereas cortical granule exocytosis occurs at anaphase I, raised the possibility that the permeability barrier and the cortical granule-derived inner eggshell layer are not the same structure. To visualize the location of the permeability barrier, we incubated embryos in solutions containing two different fluorescent small molecules, Oregon green phalloidin (molecular mass = 1,300 D) or fluorescein (molecular mass = 389 D). In both cases, the dye penetrated into the perivitelline space but, in many regions, was observed to stop short of the embryo surface (Fig. 5 A, yellow arrows). This analysis suggested that the permeability barrier is a separate structure that lies between the inner layer of the eggshell and the embryo plasma membrane. mCherry::CPG-2, which is extruded into the perivitelline space at anaphase of meiosis I, was confined to the portion of the perivitelline space outside the permeability barrier, making it an excellent marker for barrier location (Fig. 5 B). The permeability barrier could also be visualized in high contrast differential interference contrast (DIC) images (Fig. 5 B).

To identify a structure corresponding to the permeability barrier at the ultrastructural level, we performed correlative light and electron microscopy on embryos expressing mCherry::CPG-2. Fluorescence images of mCherry::CPG-2 were collected, and the embryo was immediately high-pressure frozen and processed for electron microscopy (Pelletier et al., 2006). Comparison of the fluorescence and electron microscopy images revealed that the boundary of mCherry::CPG-2 diffusion correlated with a structural boundary that partitioned space between the embryo surface and eggshell into two regions (Fig. 5 C). We propose naming the region between the embryo plasma membrane and the permeability barrier the "periembryonic space" to distinguish it from the perivitelline space between the permeability barrier and eggshell (Fig. 5 C). Consistent with its formation at anaphase of meiosis II, the permeability barrier encased the second polar body but not the first (Fig. 5 D). Live imaging of embryos expressing mCherry::CPG-2 revealed that the permeability barrier is more malleable than the eggshell. However, the permeability barrier does not always conform to the surface of the embryo. For example, when the embryo changes shape during cytokinesis, the furrow pulls away from the permeability barrier, which behaves like a tightly drawn blanket encasing the embryo (Fig. 5 E and Video 6).

To compare the properties of the periembryonic and perivitelline spaces, we analyzed the diffusion of mCherry::CPG-2. To deliver mCherry::CPG-2 to the periembryonic space where it is normally not present, we depleted KCA-1, a kinesin cargo adaptor, whose depletion leads to a partially penetrant permeable eggshell phenotype (Carvalho et al., 2011). In *kca-1(RNAi)* embryos, targeting of cortical granules to the cell surface is impaired (Video 7), causing some granules to be exocytosed at anaphase of meiosis I but a small fraction to be exocytosed after formation of the permeability barrier at anaphase II. We used partial *kca-1(RNAi)* to deliver some mCherry::CPG-2 to the periembryonic space while retaining the integrity of the permeability barrier (Fig. 5 F, area between green and yellow lines). FRAP analysis revealed that mCherry::CPG-2 in the periembryonic space recovered with similar kinetics to mCherry::CPG-2 in the perivitelline space ($t_{1/2} = 8 \pm 2.6$ s SD, $n = 7$; vs. $t_{1/2} = 8 \pm 1.8$ s, $n = 10$; Figs. 5 G and S2), suggesting that both are fluid-filled spaces with similar properties. These results show that although

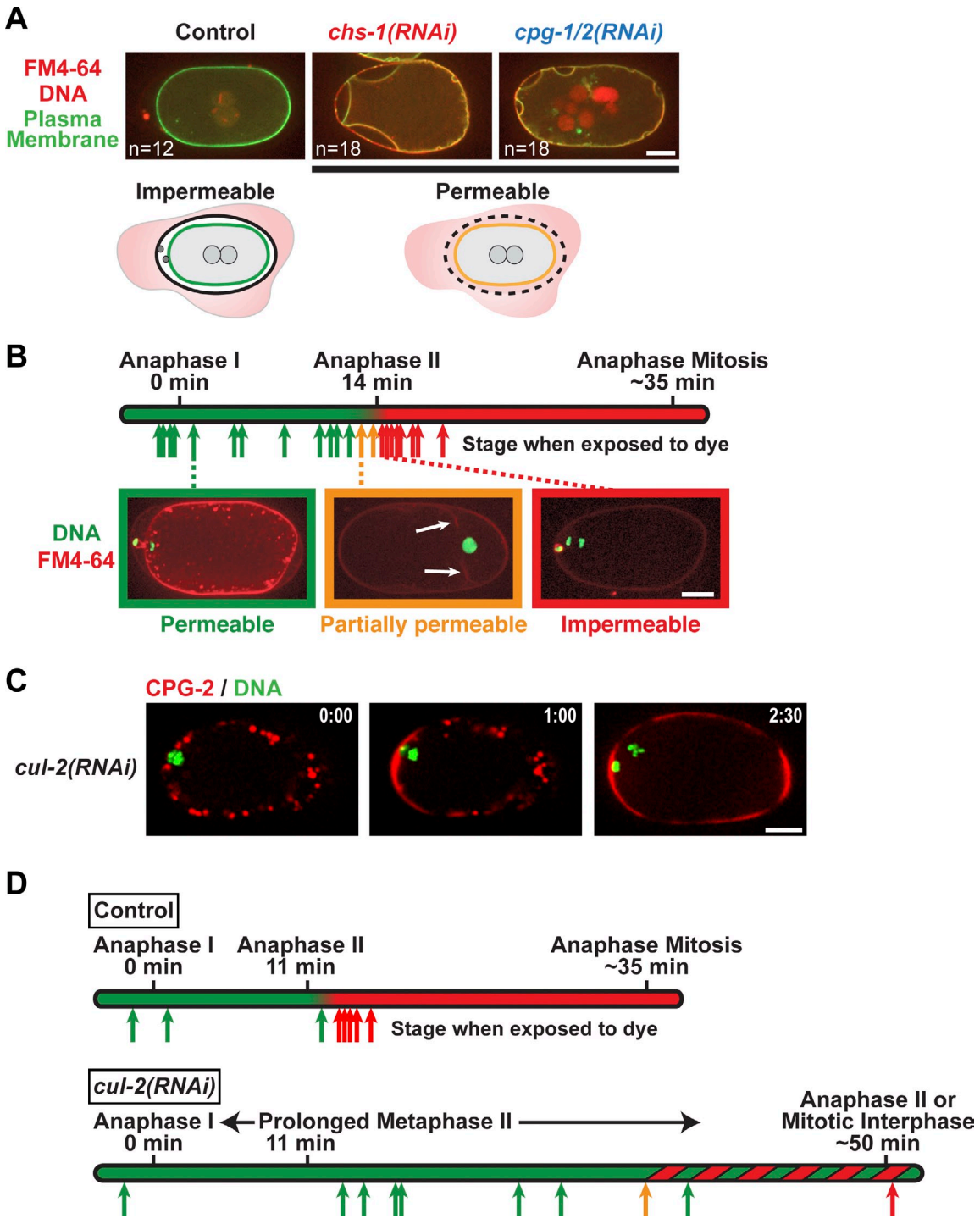

Figure 4. **Formation of a functional permeability barrier requires passage through anaphase of meiosis II.** (A) Confocal images of control (*n* = 12), *chs-1(RNAi)* (*n* = 18), and *cpg-1/2(RNAi)* (*n* = 18) embryos expressing a GFP-labeled plasma membrane probe and mCherry::histone H2B (red) that were dissected into FM4-64 dye (illustrated in schematics). (B) Embryos expressing GFP::histone H2B (green) were dissected in FM4-64 dye at different stages between anaphase of meiosis I and anaphase of the first mitotic division. Arrow positions indicate the times when that embryo was exposed to dye, and the color indicates whether it was permeable. White arrows highlight weak FM4-64 staining of the plasma membrane in a partially permeable embryo. (C) Time-lapse confocal images of a *cul-2(RNAi)* embryo expressing mCherry::CPG-2 and GFP::histone H2B (*n* = 19). Times are minutes and seconds past anaphase I. (D) Control (top; *n* = 8) and *cul-2(RNAi)* (bottom; *n* = 44) embryos expressing GFP::histone H2B and GFP::γ-tubulin were exposed to FM4-64 dye at different stages to assess eggshell permeability. Arrow positions indicate the time when that embryo was exposed to dye, and the color indicates permeability status. Embryos observed during this experiment whose temporal staging was imprecise are represented by the green and red striped region of the timeline rather than arrows (21 permeable, 2 partially permeable, and 11 impermeable embryos). Bars, 10 µm.

mCherry::CPG-2 cannot diffuse past the permeability barrier from the perivitelline space, it can diffuse freely inside the perembryonic space if delivered from the inside of the embryo. We conclude that the permeability barrier is a thin impenetrable envelope that partitions the space between the eggshell and the plasma membrane when it forms at anaphase of meiosis II.

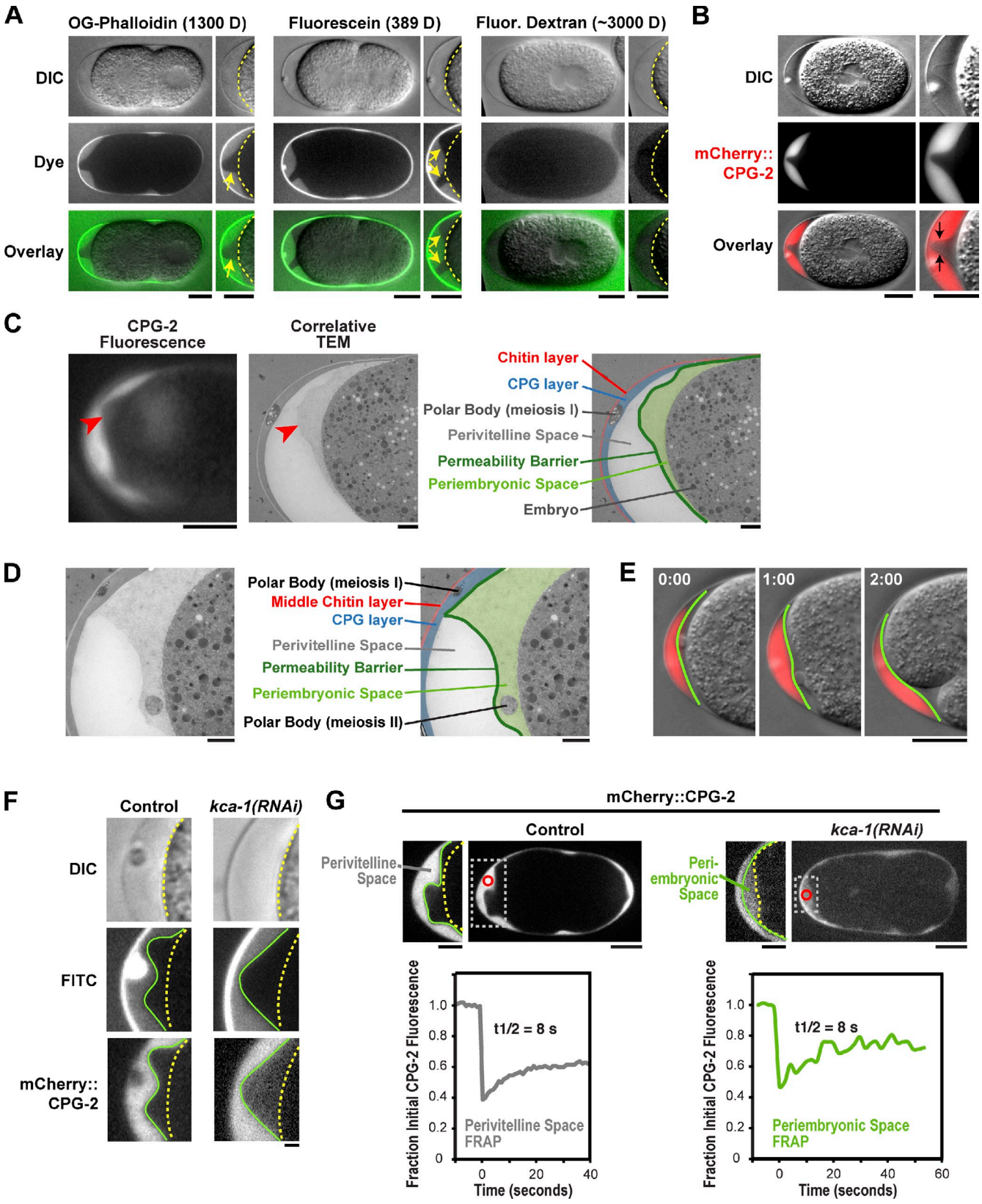

Figure 5. **The permeability barrier is a distinct envelope that forms between the embryo surface and trilaminar eggshell.** (A) Embryos placed in Oregon green (OG) phalloidin (left; *n* = 14), fluorescein (middle; *n* = 7), or 3,000-D fluorescein dextran (right; *n* = 10) were imaged by differential interference contrast (DIC; top row) and fluorescence (middle row; green in merge) microscopy. Magnified views of the embryo anterior are shown on the right (yellow dashed lines mark the embryo plasma membrane; yellow arrows point to the edge of the permeability barrier). (B) DIC (top) and fluorescence (middle; red in merge) images of a one cell–stage mitotic embryo expressing mCherry::CPG-2 (*n* = 9). The embryo anterior is magnified on the right. The contrast of the top DIC image has been adjusted to visualize the edge of the permeability barrier (indicated by the black arrows in the merge). (C, left) A fluorescence

Genes involved in fatty acid synthesis are required to form the permeability barrier

Depletion of enzymes required for fatty acid biosynthesis and modification, including POD-2 (acetyl-CoA carboxylase), FASN-1 (fatty acid synthase), EMB-8 (NADPH-cytochrome P450 reductase), and CYP-31A2/CYP-31A3 (cytochrome P450s; Fig. 6 A) have been shown to result in the Pod (polarity and osmotic defective) phenotype and have been proposed to be required for assembly of the inner eggshell layer (Tagawa et al., 2001; Rappleye et al., 2003; Benenati et al., 2009). Given our finding that the inner eggshell layer is not the permeability barrier, we hypothesized that depletion of these genes affects formation of the permeability barrier rather than of the inner eggshell layer. Consistent with this idea, depletion of fatty acid biosynthetic/modification enzymes did not affect chitin or mCherry::CPG-1 localization (Fig. 6 B), and no membrane scalloping or eggshell rupture phenotypes associated with defects in the chitin and inner eggshell layers were observed (Fig. 6 C). In contrast, when fatty acid enzymes were inhibited, the permeability barrier was compromised—FM4-64 dye bound the plasma membrane and mCherry::CPG-2 freely diffused within the entire space between the eggshell and the plasma membrane (Fig. 6 B). Thus, the fatty acid biosynthetic pathway is required for formation of the permeability barrier in a step that occurs after the assembly of the trilaminar eggshell.

To determine whether the fatty acids used in eggshell formation are synthesized in the germline or whether the germline imports fatty acids synthesized in another tissue, such as the intestine, we performed RNAi in *rrf-1(pk1417)* mutant worms in which germline RNAi is intact, but somatic RNAi is defective. For all genes tested, embryos failed to form a permeability barrier when RNAi was only effective in the germline (Fig. 7), indicating that the fatty acid derivatives comprising the permeability barrier are synthesized by germline-expressed enzymes.

A requirement for PERM-1 and DGTR-1 suggests that the fatty acid required for permeability barrier formation is an ascaroside

We recently performed an RNAi screen for genes involved in *C. elegans* eggshell assembly (Carvalho et al., 2011) that implicated two previously uncharacterized genes, *perm-1* (permeable eggshell) and *dgtr-1* (*DGAT* related), as important for assembly of an impermeable eggshell. Using the aforementioned assays, we determined which step of eggshell assembly is affected by inhibition of PERM-1 or DGTR-1. This analysis revealed that depletion of PERM-1 or DGTR-1 phenocopies inhibition of the fatty acid synthesis genes. Depleted embryos showed normal localization of the chitin probe and mCherry::CPG-1, but the permeability barrier was compromised (Fig. 8 A). PERM-1 and DGTR-1 are required in the germline, similar to the fatty acid genes (Fig. 8 B). Primary sequence analysis of PERM-1 revealed homology to dehydratase, NAD binding, nucleotide sugar epimerase, and dehydrorhamnose reductase protein domains (Fig. 8 C), all of which would be required to generate the nucleotide sugar cytidine diphosphate (CDP)-ascarylose from a CDP-glucose precursor (Thibodeaux et al., 2007). Ascarylose is a rare dideoxy sugar found in ascaroside glycolipids, which are comprised of one or two ascarylose sugars covalently attached to a long-chain fatty acid–like molecule (Fig. 8 D). Ascarosides were previously purified from the eggshells of parasitic nematode species (Timm, 1950; Fouquey et al., 1957; Jezyk and Fairbairn, 1967; Tarr and Fairbairn, 1973; Bartley et al., 1996), and *C. elegans* is known to make short chain ascarosides, such as dauer pheromone, that perform signaling functions (Butcher et al., 2009; Edison, 2009). DGTR-1 shows homology to the DGAT2 family of acyl-CoA:diacylglycerol acyltransferase enzymes, which catalyzes the addition of fatty acyl-CoA to diacylglycerol to form triacylglycerol. The chemical reaction catalyzed by DGAT2 is similar to that expected to covalently link ascarylose to long-chain fatty acids, suggesting that DGTR-1 may also be implicated in ascaroside biosynthesis (Fig. 8 D). The identification of the sugar-modifying enzyme PERM-1 and the acyl chain transfer enzyme DGTR-1 as important for permeability barrier formation suggests that a glycolipid, perhaps an ascaroside, is an essential component of the permeability barrier.

Discussion

The work described here shows that the *C. elegans* zygote builds a trilaminar eggshell consisting of an outer vitelline layer that is present on the oocyte surface before fertilization, a middle chitin-containing layer that is assembled immediately after fertilization, and an inner layer containing the CPG-1/2 proteoglycans that forms concurrent with cortical granule exocytosis at anaphase of meiosis I. Assembly of the trilaminar shell is followed by a distinct step during anaphase of meiosis II that builds a malleable envelope that functions as a permeability barrier; this step requires fatty acid and carbohydrate synthesis/

image of CPG-2 was acquired immediately before cryoimmobilization and processing for transmission electron microscopy (n = 3). (middle) Alignment of the resulting correlative transmission electron micrograph (TEM) image allows visualization of the edge of the permeability barrier (red arrowheads). (right) A pseudocolored micrograph illustrates the location of the chitin and CPG eggshell layers along with the edge of the permeability barrier. The periembryonic and perivitelline spaces and the first polar body are also labeled. (D) Transmission electron micrographs of a control embryo showing the location of the polar bodies extruded during anaphase of meiosis I (embedded in the CPG layer; see also C) and during anaphase of meiosis II (in the periembryonic space). (E) Merged DIC and fluorescence images of the anterior of an embryo at the two-cell stage expressing mCherry::CPG-2. Green lines mark the location of the permeability barrier. Time indicates minutes and seconds past the first frame. (F) DIC and confocal fluorescence images of control (n = 12) and partial *kca-1(RNAi)* (n = 12) embryos expressing mCherry::CPG-2. (middle row) Embryos were also exposed to FITC dye to monitor the integrity of the permeability barrier (green lines). The embryo surface is also marked (dashed yellow lines). (G) Confocal fluorescence images of control (left) and partial *kca-1(RNAi)* (right) embryos expressing mCherry::CPG-2. The mCherry::CPG-2 in the perivitelline (left) or periembryonic (right) spaces was photobleached (red circle inside dashed white box, magnified on the left) at 0 s, and the embryo was continuously imaged every 1 or 2 s (left and right, respectively) to monitor recovery (quantified in graphs below). Bars: (A–C [left], E, and G) 10 µm; (C [middle and right], D, and F) 1 µm.

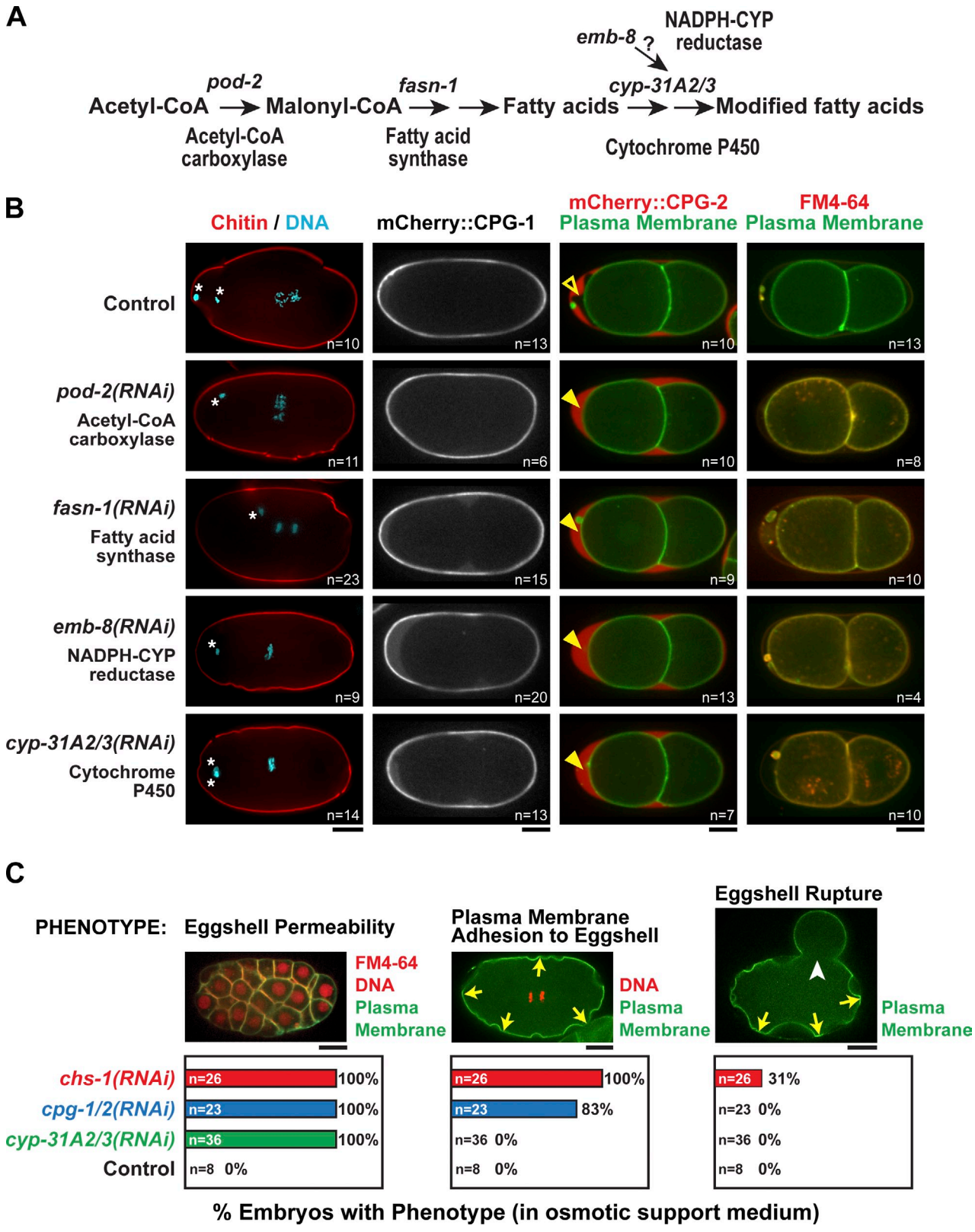

Figure 6. **Genes involved in fatty acid synthesis are required to form the permeability barrier.** (A) Schematic outline of some of the genes in the fatty acid biosynthetic and modification pathway. CYP, Cytochrome P450. (B) Confocal images of control embryos and embryos in which the indicated proteins were inhibited by RNAi. (first column) The middle chitin layer was visualized in fixed embryos by staining for chitin and DNA. White asterisks mark extruded polar bodies. (second column) The inner CPG layer was visualized in embryos expressing mCherry::CPG-1. (third column) The presence of the permeability barrier was assessed in embryos expressing mCherry::CPG-2 and a GFP-tagged plasma membrane marker. In control embryos, the permeability barrier prevents diffusion of mCherry::CPG-2 to the embryo surface (open arrowhead). When fatty acid synthesis is inhibited, the permeability barrier is disrupted, and mCherry::CPG-2 fills the entire space between the eggshell and embryo surface (closed arrowheads). (last column) Embryos expressing a GFP-tagged

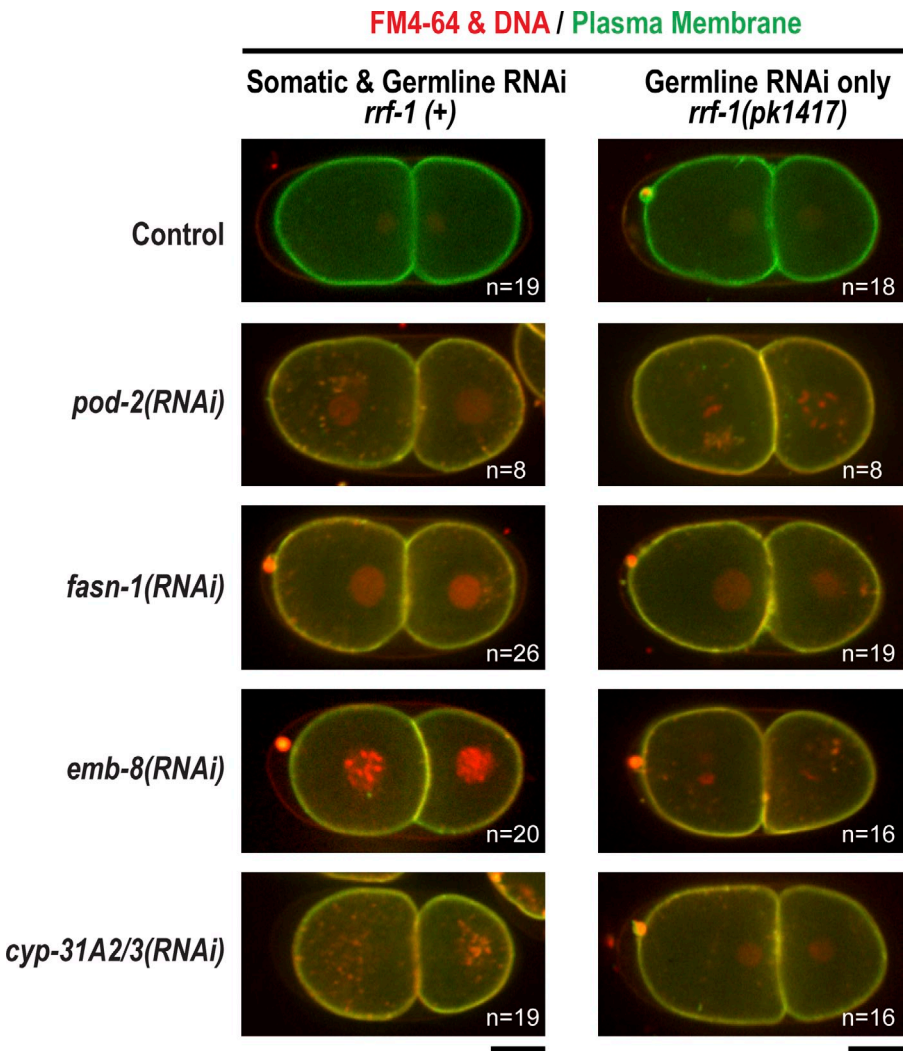

Figure 7. **Permeability barrier formation requires germline expression of fatty acid synthesis genes.** Confocal images of control embryos and embryos in which the indicated components of the fatty acid biosynthesis pathway were inhibited by RNAi in either an *rrf-1(+)* (left) or *rrf-1(pk1417)* mutant background (right). Embryos expressing a GFP-tagged plasma membrane probe and mCherry::histone H2B (red) were placed in FM4-64 dye. All RNAi-treated embryos were permeable in the *rrf-1(pk1417)* background, indicating that germline expression of these genes is required. *n* = number of imaged embryos. Bars, 10 µm.

modification enzymes, suggesting that this internal envelope contains glycolipids. The chitin layer provides mechanical rigidity and serves as a block to polyspermy; the inner CPG layer prevents plasma membrane adhesion to the chitin layer and expands the fluid-filled perivitelline space, and the permeability barrier isolates the embryo from the environment. Collectively, the trilaminar shell and permeability barrier provide a protective environment for embryo development.

We propose the nomenclature in Fig. 9 for the eggshell layers, permeability barrier, and intervening spaces. The outer vitelline layer, which covers the oocyte surface before fertilization, was originally named by Foor (1967), and we favor retaining this term as it corresponds to the names for the analogous initial ECM layer in other species (vitelline layer in echinoderms, vitelline envelope in amphibians, mollusks, and crustaceans, and vitelline membrane in dipterans; Wong and Wessel, 2006). We propose the term chitin layer to describe the middle layer of the trilaminar shell because immunoelectron microscopy demonstrated that chitin is present in and limited to this middle layer. The innermost layer of the eggshell was previously termed the lipid-rich layer, but our data suggest that this layer is instead comprised of cortical granule cargo. We propose naming this layer the CPG layer after its essential structural components, CPG-1/2. We propose naming the impermeable barrier between the eggshell and embryo surface the permeability barrier. The space between the embryo plasma membrane and the eggshell has been previously termed the perivitelline space. As the permeability barrier partitions this space into two distinct compartments, we propose using the term perivitelline space for the region between the eggshell and the permeability barrier and the term periembryonic space for the

plasma membrane probe were placed in FM4-64 dye to test their permeability. (C) The phenotypic consequences of disrupting the eggshell permeability barrier (*cyp-31A2/3(RNAi)*), the inner CPG layer (*cpg-1/2(RNAi)*), and the middle chitin layer (*chs-1(RNAi)*) were compared by analyzing the percentage of embryos exhibiting each of the indicated phenotypes. Data were pooled from >10 independent imaging sessions for each condition. Plasma membrane adhesion (yellow arrows) was also usually accompanied by cytokinesis failure (59% of *cpg-1/2(RNAi)* embryos failed cytokinesis). In addition to the quantified phenotypes, chitin layer disruption also led to polyspermy (24% of *chs-1(RNAi)* embryos were polyspermic). The images of embryos illustrating membrane adhesion and eggshell rupture (white arrowhead) are reproduced from Fig. 3 B. The left image is of an embryo expressing a GFP-tagged plasma membrane marker and mCherry::histone H2B (red) that was placed in FM4-64 dye. Bars, 10 µm. *n* = number of imaged embryos.

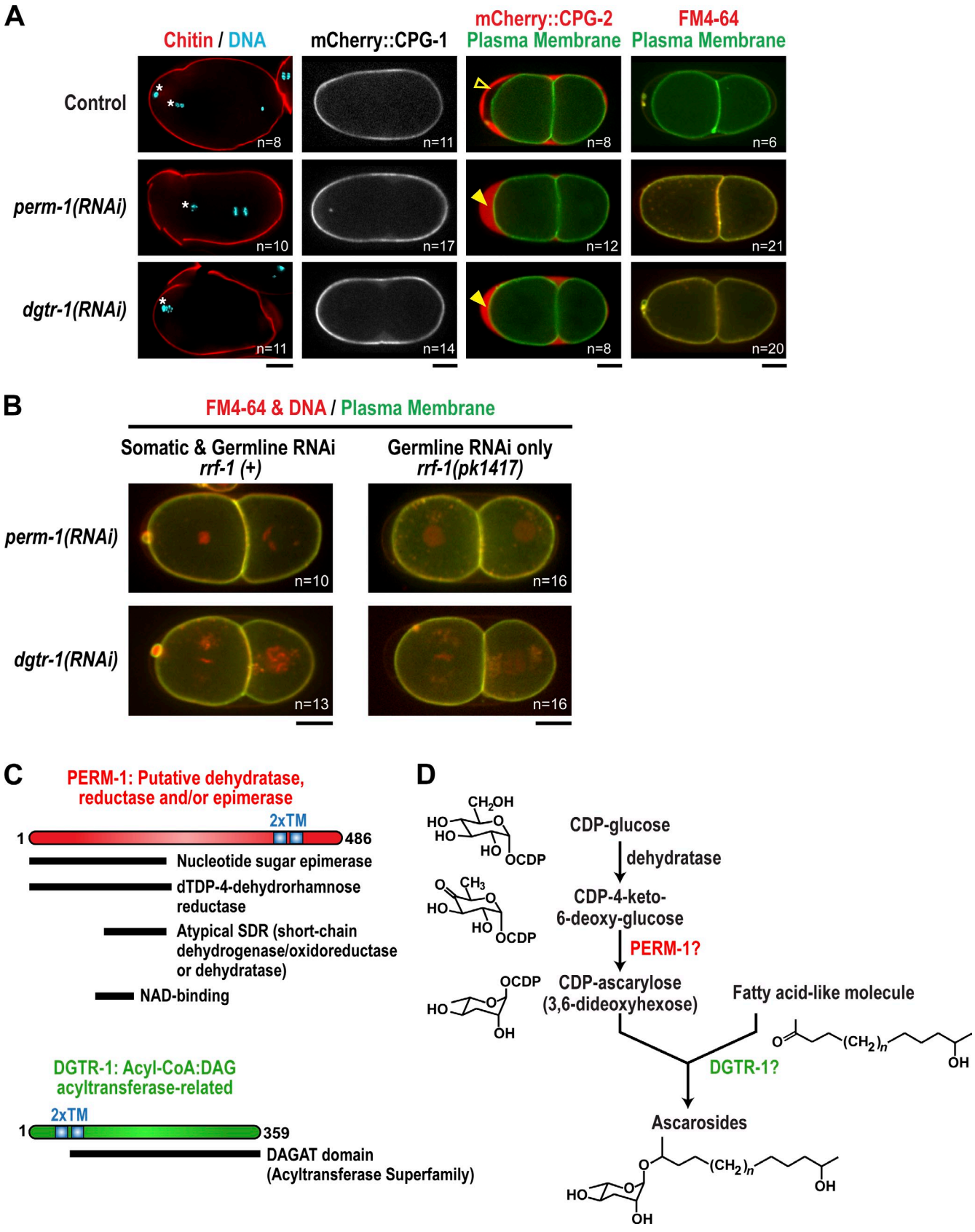

Figure 8. **A requirement for PERM-1 and DGTR-1 suggests that an ascaroside may be important for permeability barrier formation.** (A) Confocal images of control embryos and embryos in which PERM-1 and DGTR-1 were depleted by RNAi. (first column) The middle chitin layer was visualized in fixed embryos by staining for chitin and DNA. White asterisks mark extruded polar bodies. (second column) The inner CPG layer was visualized in embryos expressing mCherry::CPG-1. (third column) The presence of the permeability barrier was assessed in embryos expressing mCherry::CPG-2 and a GFP-tagged plasma

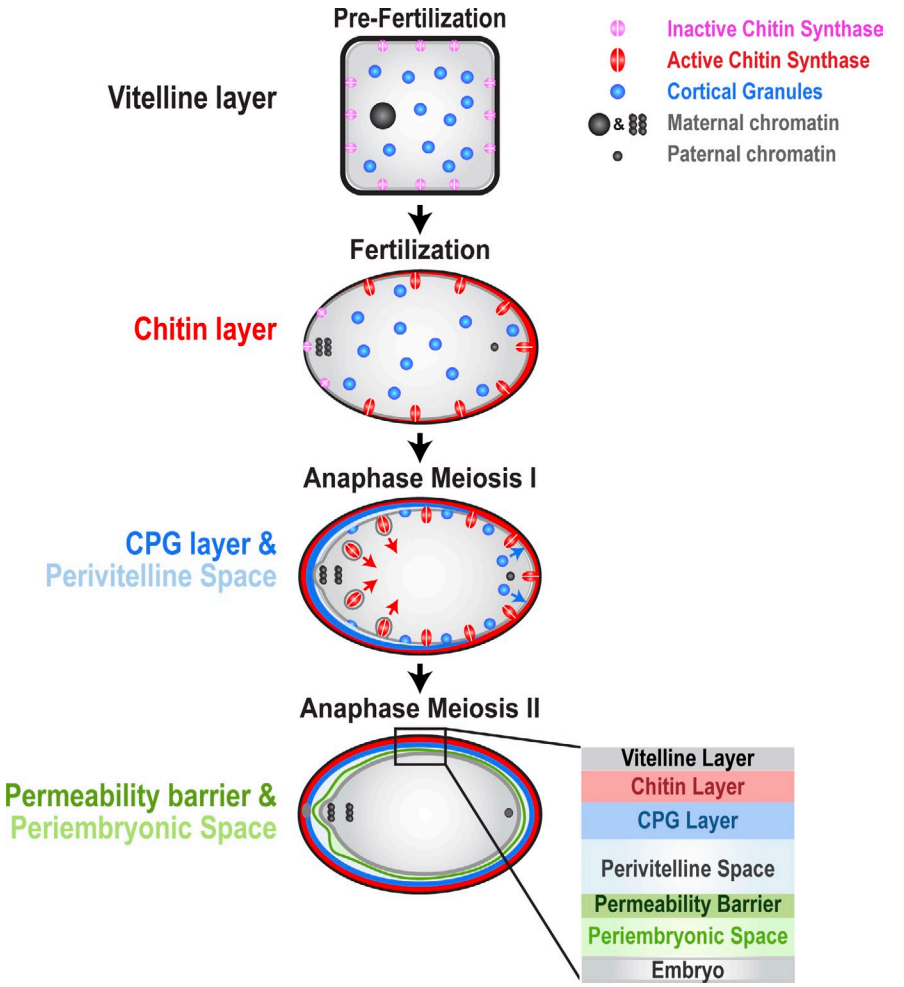

Figure 9. **Model for assembly of the *C. elegans* eggshell and permeability barrier.** Schematic outline of sequential steps in assembly of the eggshell and permeability barrier. The plasma membrane of prefertilization oocytes is coated with an electron-dense vitelline layer. Fertilization activates chitin synthase, which deposits a chitin layer between the vitelline layer and plasma membrane. At anaphase of meiosis I, cortical granules containing CPG-1 and CPG-2 are exocytosed in a wave that proceeds from the anterior (left) to the posterior (right) of the embryo. As cortical granules are exocytosed, the CPG layer is deposited, and a perivitelline space opens up between the plasma membrane and eggshell. Chitin synthase is internalized from the embryo surface after the onset of cortical granule exocytosis. At anaphase of meiosis II, fatty acid derivatives, possibly ascarosides, assemble between the eggshell and the embryo surface to form the permeability barrier. Between the permeability barrier and the embryo surface is the periembryonic space, which receives the contents of vesicles exocytosed after anaphase of meiosis II.

region between the permeability barrier and embryo plasma membrane. The slightly more electron-dense region around the embryo was observed in a previous study and termed the embryonic layer (Benenati et al., 2009), as it was thought to be a layer of ECM surrounding the embryo. Our data showing that the embryo can pull away from this layer when it changes shape during cell division and analyzing the diffusion of mCherry::CPG-2 indicate that, rather than being an ECM layer, this region is a fluid-filled space containing soluble proteins that is bounded by the permeability barrier; we therefore prefer the term periembryonic space for this region. This nomenclature reflects the characteristics of each layer and provides a consistent framework for investigation of the molecular mechanisms driving assembly of the postfertilization ECM.

Chitin and the CPG-1/2 proteoglycans define the middle and inner eggshell layers

CPG-1 and CPG-2 contain chitin-binding domains similar to those in the peritrophins, which form a semipermeable gelatinous mixed matrix comprised of chitin and proteoglycans that lines the insect gut (Lehane, 1997). Based on this precedent, we had expected that either the middle or inner eggshell layers would be a composite matrix made up of chitin and CPG-1/2. Instead, our data indicate that chitin is restricted to the middle layer, and CPG-1/2 is restricted to the inner layer. This suggests that rather than allowing formation of a mixed matrix within an eggshell layer, the chitin-binding domains in CPG-1/2 serve to recruit them to the interface between the chitin and CPG layers.

membrane marker. In control embryos, the permeability barrier prevents diffusion of mCherry::CPG-2 to the embryo surface (open arrowhead). When PERM-1 and DGTR-1 are inhibited, mCherry::CPG-2 fills the entire space between the eggshell and embryo surface (closed arrowheads). (last column) Embryos expressing a GFP-tagged plasma membrane probe were placed in FM4-64 dye to test their permeability. (B) Confocal images of embryos in which PERM-1 and DGTR-1 were inhibited by RNAi in either an *rrf-1(+)* (left column) or *rrf-1(pk1417)* mutant background (right column). Embryos expressing a GFP-tagged plasma membrane probe and mCherry::histone H2B (red) were placed in FM4-64 dye to test their permeability. For A and B, *n* = number of imaged embryos. Bars, 10 µm. (C) Schematics of PERM-1 and DGTR-1 showing the location of domains predicted by BLAST (Basic Local Alignment Search Tool). The TOPCONS program (Stockholm Bioinformatics Center) predicted both proteins to contain two transmembrane domains (2×TM). dTDP, deoxythymidine diphosphate. (D) A putative pathway for ascaroside synthesis in which activated CDP-ascarylose (left side) combines with a long-chain fatty acid–like molecule (right side) to generate ascaroside glycolipid. The reactions proposed to convert CDP-glucose into CDP-ascarylose are based on chemical reactions identified in prokaryotes (Thibodeaux et al., 2007). Points where PERM-1 and DGTR-1 might function in this pathway are indicated.

We show that CPG-1 and -2 are redundantly required for assembly of the inner eggshell layer and for separation of the chitin-containing shell from the plasma membrane to open up the perivitelline space. We propose that this occurs through binding of CPG-1/2 to the middle chitin layer, relieving adhesion between the eggshell and embryo surface. The osmotic gradient generated by the polyanionic chondroitin chains and their counterions might then drive a hydration reaction that transfers water from the embryo to the perivitelline space. Although CPG-1 anchored within the inner layer is sufficient to drive this reaction, the freely diffusible population of CPG-2 in the perivitelline space might also contribute. The proteoglycan hydration reaction we propose is similar to the reaction previously proposed to lift the vitelline layer from the plasma membrane in sea urchin embryos. In that case, cortical granules deliver glycosaminoglycans that hydrate upon release, providing hydrostatic force that lifts the rapidly expanding vitelline layer (Schuel et al., 1974; Wong and Wessel, 2008). This similarity suggests general conservation of the mechanisms used to drive layer separation during the formation of extracellular coverings.

The permeability barrier maintains two distinct fluid-filled microenvironments between the embryo and shell

The trilaminar shell does not block entry of small molecules but does prevent the entry/exit of larger molecules, such as 3,000-D fluorescent dextran (Fig. 5 A). The trilaminar eggshell may thus serve as a filter to prevent the entry of larger proteins/molecules from the environment or, perhaps more significantly, to allow retention of exocytosed molecules, such as CPG-2, within the perivitelline space. The more stringent permeability barrier is formed by a distinct envelope built at anaphase of meiosis II and encases the embryo. The perivitelline space contains proteins exocytosed before anaphase of meiosis II, whereas proteins exocytosed after anaphase of meiosis II are retained in the periembryonic space by the permeability barrier. The presence of two concentric fluid-filled spaces, the perivitelline space and the periembryonic space, may provide an ideally cushioned and buffered environment for embryonic development.

This view explains a previously puzzling observation that embryos depleted of POD-1, a coronin that regulates both the actin cytoskeleton and membrane trafficking, possess an extra eggshell layer adjacent to the embryo surface in electron microscopy images (Rappleye et al., 1999). By imaging mCherry::CPG-2, we found that although some cortical granules were exocytosed at anaphase I in *pod-1(RNAi)* embryos, the exocytosis of other granules was delayed until after anaphase of meiosis II (Video 8). Thus, *pod-1(RNAi)* embryos form two CPG layers, one based on exocytosis at the normal time and the second based on exocytosis after formation of the permeability barrier.

In addition to protecting the embryo by maintaining proper osmotic conditions and preventing the entry of potentially harmful small molecules from the environment, the permeability barrier may also allow the embryo to maintain secreted molecules that signal between embryonic cells in close proximity. This could explain in part why disrupting the eggshell permeability barrier ultimately prevents normal development (Schierenberg and Junkersdorf, 1992; Lee and Goldstein, 2003; Carvalho et al., 2011).

The composition of the permeability barrier

Our work implicates enzymes required for fatty acid synthesis, sugar modification, and acyl chain transfer in the formation of the permeability barrier, suggesting that a key component of this layer may be a glycolipid. Consistent with this, early observations in *Parascaris equorum* demonstrated that the permeability barrier was composed of a fatty material with a melting point of 72°C (Fauré-Fremiet, 1913). The fatty component was later extracted from *Ascaris lumbricoides* and *Meloidogyne javanica* and found to be very similar in properties to beeswax (Chitwood, 1938; Christenson, 1950; Timm, 1950). Subsequent biochemical characterization identified ascarosides, long-chain fatty acids with a head group containing one or two ascarylose sugars, as the major lipid component of the permeability barrier in *A. lumbricoides* species (Timm, 1950; Fouquey et al., 1957; Jezyk and Fairbairn, 1967; Tarr and Fairbairn, 1973; Bartley et al., 1996). Although the lipids that make up the *C. elegans* permeability barrier have not yet been characterized, ascarosides remain attractive candidates. *C. elegans* is known to make ascarosides with fatty acid chains of varying lengths. Short fatty acid chain ascarosides act as pheromones that promote mating and the dauer state (Butcher et al., 2009; Edison, 2009). A recent study reported the isolation of two long-chain ascarosides from *C. elegans* but did not find a role for these lipids in eggshell impermeability or dauer formation (Zagoriy et al., 2010). The enzymatic machinery specifically required for ascaroside biosynthesis is largely uncharacterized. We recently performed a functional screen that identified components required for embryo impermeability (Carvalho et al., 2011). Among the components identified by this screen were PERM-1 and DGTR-1. The analysis we perform here specifically implicates these enzymes in formation of the permeability barrier, and their domain structure strongly suggests a potential function in the ascaroside synthesis pathway.

In addition to its molecular composition, a second important question is how the permeability barrier is formed. The permeability barrier forms after the trilaminar shell, presumably by secretion of lipids from the embryo. Lipids could accumulate on a protein scaffold on the inner eggshell layer and then peel off to form a separate layer, or they could accumulate on a protein scaffold on the embryo surface and subsequently lift up to form a separate layer. The observation that CPG-2 remains strictly outside of the permeability barrier after it forms causes us to favor the latter view because CPG-2 is exocytosed before permeability barrier formation and diffuses freely within the perivitelline space.

Placing the new view of eggshell and permeability barrier formation in a historical context

Investigation of the nematode eggshell has a rich history dating back to 1850. Light microscopy-based experiments of the eggshells of >40 nematode species conducted between 1850

and 1950 are summarized in a chapter by Christenson (1950) in the classical book "An Introduction to Nematology." These early observations partitioned the nematode eggshell into two key parts, a chitin-containing "true shell" that conferred mechanical rigidity (Krakow, 1892; Chitwood, 1938; Christenson, 1950) and an inner curtainlike layer termed the vitelline membrane that constituted the eggshell permeability barrier (Christenson, 1950). Concurrent with the use of electron microscopy to characterize nematode eggshells in a variety of species, this bipartite view was replaced with the idea of a single trilaminar shell composed of an outer vitelline layer (distinct from the vitelline membrane in the original view), a middle chitin layer, and an inner lipid-rich layer (also called the ascaroside layer; Rogers, 1956; Foor, 1967; Bird, 1971; Wharton, 1980). In this modern view, the permeability barrier was the inner layer of the trilaminar shell, rather than a distinct membrane between the eggshell and the embryo surface (Wharton, 1980; Mansfield et al., 1992; Rappleye et al., 1999; Bembenek et al., 2007; Benenati et al., 2009).

Our results using correlative light and electron microscopy demonstrate that the permeability barrier is not the inner layer of the trilaminar shell but a separate envelope akin to the vitelline membrane described in the older work. We show that fatty acid synthesis/modification enzymes are required for formation of the permeability barrier, suggesting that the permeability barrier, rather than the inner layer of the trilaminar shell, contains lipids. The idea of a separate vitelline membrane was lost coincident with the advent of studies examining the eggshell by electron microscopy (Rogers, 1956; Foor, 1967; Bird, 1971; Wharton, 1980), likely caused by the difficulty in preserving and identifying this structure in chemically preserved specimens. The large body of work on nematode eggshells highlights intriguing similarities in eggshell formation across nematode species, suggesting that dissecting eggshell formation in *C. elegans* will provide insights that will be useful in combating parasitic species.

Materials and methods

C. elegans strains

All strains (genotypes listed in Table S1) were maintained at 20°C. The *cpg-1* and *cpg-2* deletion mutants were outcrossed 6× before analysis and marker introduction. The strains OD58 (GFP plasma membrane marker; Audhya et al., 2005), TH32 (GFP::histone H2B and GFP::γ-tubulin; Desai et al., 2003), AZ212 (GFP::histone H2B; Praitis et al., 2001), and AD265 (GFP::CHS-1; Maruyama et al., 2007) have been described previously. MSN-100 (GFP::CAV-1), which is similar to the strain originally described in Sato et al. (2006), was a gift of A. Audhya (University of Wisconsin, Madison, WI). Fluorescent proteins were expressed from the *pie-1* promoter and 3′ untranslated region regulatory elements. Some nematode strains used in this work were provided by the Caenorhabditis Genetics Center, which is funded by the National Institutes of Health National Center for Research Resources.

Plasmids and transgenic strains

N-terminal mCherry expression constructs were engineered starting from pIC26 (Cheeseman et al., 2004). The *pie-1* 5′ and 3′ regulatory information and GFP coding sequence were removed by digesting pIC26 with NotI, religating, then digesting with BamHI and KpnI, and religating after blunting with the Klenow large fragment (New England Biolabs, Inc.). mCherry preceded by the CPG-1 signal peptide sequence was introduced by using the primer pairs 5′-GCGGCCGCGGTACCACTCTCAAGCCAGTTCTTCTTGCATTCCTTGTTGCATCGGCCTACGCAATGGTCTCAAAGGGTGAAGAAGAT-3′ and 5′-GCGGCCGCCTTATACAATTCATCCATGCCACC-3′ to amplify mCherry from pAA65 (McNally et al., 2006) and cloning this into the NotI site to generate plasmid pSO22. The plasmids pSO31 and pSO33, which encode mCherry::CPG-1 (5′-GGTACCGAATTTCAACCTTCATGCTCGAACTTATTCG-3′, 5′-GGTACCCATCCTACTGAAAATAGAAATTCAATAGGGT-3′, 5′-ACTAGTGGTGTAGCTGGAATGTATGAGAATCTGCCA-3′, and 5′-ACTAGTCTCCATCCACACAAAAATCACCAGCTG-3′) and mCherry::CPG-2 (5′-GGTACCGTGCCTCATGAACTTTCGGCATCA-3′, 5′-GGTACCCATCCTCCTGAAATAAAGATCTTTAAGAAAAGAGAACAA-3′, 5′-ACTAGTCAGTTCCTTCAAGACTGTACAAACGC-3′, and 5′-ACTAGTGGGTCGCAATTGAGGCTTTTACCACTC-3′), respectively, were generated by using the primer pairs in parentheses to amplify the promoters and ORFs/3′ untranslated regions from genomic DNA and cloning into the KpnI and SpeI sites of pSO22. The SpeI site in the *cpg-1* promoter was mutated from ACTAGT to ACTAGG before cloning using the mutagenesis kit (QuikChange II; Agilent Technologies).

Transgenic lines were created by microparticle bombardment of pSO31 and pSO33 (Praitis et al., 2001). For each bombardment, 6 mg of 2.0-µm gold beads were placed in a siliconized 1.5-ml microfuge tube. Beads were sequentially washed with 1 ml of 70% ethanol and 1 ml double-distilled H_2O. For each wash, the beads were vortexed for 5 min, allowed to settle for 1 min, and spun in a microfuge for ∼5 s before removing the supernatant. Beads were resuspended in 100 µl of 50% glycerol and vortexed for 5 min. 10 µl plasmid DNA at a concentration of 1–2 mg/ml was added, and the tube was vortexed for 60 s. 100 µl of 2.5-M $CaCl_2$ was added, and the tube was vortexed for 60 s. 40 µl of 0.1-M spermidine was added, and the tube was vortexed for 3 min. Beads were settled for 1 min and spun in a minimicrofuge for ∼5 s, and the supernatant was removed. 300 µl of 70% ethanol was added, the beads were vortexed for 1 min, settled for 1 min, and spun in a microfuge for ∼5 s, and the supernatant was removed. 150 µl of 100% ethanol was added, and the beads were vortexed for 3 min before placing 20 µl of beads onto the center of macrocarriers (Bio-Rad Laboratories). After the solution had dried, macrocarriers were placed into an adapter (Hepta; Bio-Rad Laboratories) and used to bombard pellets of DP38 worms on a 100-mm worm plate according to the manufacturer's instructions. DP38 worms were grown on 100-mm C600/peptone plates until just starved. Worms were washed in M9, resuspended in 1 ml M9, pipetted onto spots on a 100-mm worm plate aligned with the Hepta adapter, and allowed to dry until the liquid was just absorbed. Worms rescued from paralysis because of the presence of the *unc-119(+)*–rescuing fragment in the plasmids were screened for expression of the fluorescence construct.

Antibody production

To generate antibodies to CPG-1 (5′-GAATTCGACTGTTCCACGAAGGAAGACGGAC-3′ and 5′-GCGGCCGCATTCGTGCACTCTGGAACATTCATAACG-3′) and CPG-2 (5′-GAATTCGAGCCAACATGCGAAGGAAAAGC-3′ and 5′-GCGGCCGCTTGGCATTCGGAAACATTGGACTCG-3′), the primer pairs in parentheses were used to amplify regions corresponding to amino acids 60–268 of CPG-1 and 244–360 of CPG-2 from *C. elegans* cDNA. Fragments were cloned into the EcoRI and NotI sites of pGEX6P-1 (GE Healthcare). GST fusions were purified, and the GST was removed using a fusion protein (PreScission Protease; GE Healthcare) before outsourcing the proteins for injection into rabbits (Robert Sargeant Antibodies). Antibodies were purified using standard procedures (Harlow and Lane, 1988) on a 1-ml *N*-hydroxysuccinimide HiTrap column (GE Healthcare) containing the immobilized GST fusions. The antibody raised against CPG-1 (Ab153) recognizes both CPG-1 and CPG-2, whereas the antibody raised against CPG-2 (Ab154) specifically recognizes CPG-2 (Fig. S1 A).

Immunofluorescence

Immunofluorescence was performed as previously described (Monen et al., 2005) with the following modifications. Embryos and gonads were dissected onto subbing solution-coated glass slides in 0.75× egg salts (88.5 mM NaCl, 30 mM KCl, 2.55 mM $MgCl_2$, 2.55 mM $CaCl_2$, and 3.75 mM Hepes, pH 7.4), freeze cracked, and fixed in −20°C methanol for 15 min. Slides were processed for immunofluorescence using a 1:100 dilution of rhodamine-conjugated chitin-binding probe (New England Biolabs, Inc.) or 1 µg/ml each of primary antibody (Ab153 or Ab154) followed by 1 µg/ml Cy3-labeled secondary antibody. DNA was stained with 1 µg/ml Hoechst. Images were acquired using a 100×, 1.35 NA U-Plan Apochromat oil objective lens (Olympus) and charge-coupled device (CCD) camera (CoolSNAP; Roper Scientific) mounted on a microscope

(DeltaVision; Applied Precision). Deconvolution and image processing was performed with softWoRx software (Applied Precision). DNA and gonad images are projections of multiple 2-µm z sections, whereas eggshell images are of a central plane.

RNA-mediated interference

Double-stranded RNAs (dsRNAs) were prepared by using the oligonucleotides listed in Table S2 to PCR amplify regions from N2 genomic DNA. PCR reactions were cleaned (QIAGEN) and used as templates for 50 µl T3 and T7 transcription reactions (MEGAscript; Invitrogen). Transcription products were mixed, purified by phenol-chloroform extraction, and annealed by resuspending the RNA pellet in soaking buffer (11 mM Na_2HPO_4, 5.5 mM KH_2PO_4, 2.1 mM NaCl, and 4.7 mM NH_4Cl) and incubating at 68°C for 10 min followed by 37°C for 30 min (Oegema et al., 2001; Green et al., 2011). L4-stage hermaphrodites were injected with dsRNA and incubated for 6–48 h at 16–20°C before live imaging.

Live imaging

Embryos were dissected in 4 µl of 0.7–0.8× egg salts (empirically determined daily; Tagawa et al., 2001) to provide osmotic support and filmed without compression on a 24 × 60–mm coverslip mounted on a metal holder (Monen et al., 2005). For permeability experiments, FM4-64 was added to the medium at a final concentration of 3.3–6.6 µM. To prevent compression, a ring of Vaseline was placed around the embryos, and the chamber was sealed with a 22 × 22–mm coverslip. Alternatively, for the *cul-2(RNAi)* experiment (Fig. 4 D), embryos were dissected and filmed in a microfluidics chamber (Carvalho et al., 2011). Embryos were imaged on one of three microscope systems: (1) an inverted spinning-disc confocal microscope (TE2000-E; Nikon) equipped with a solid-state laser combiner (ALC; Andor Technology) and CCD camera (Clara; Andor Technology) controlled by iQ software (Andor Technology) with 2 × 2 binning, (2) an inverted spinning-disc confocal microscope (Observer.Z1; Carl Zeiss) equipped with a CCD camera (QuantEM; Photometrics) without binning, or (3) a upright microscope (Eclipse E800; Nikon) equipped with a CCD camera (ORCA-ER; Hamamatsu Photonics) controlled by MetaMorph software (Molecular Devices) without binning. In all cases, images were acquired of a single central plane with a 60×, 1.4 NA Plan Apochromat objective lens and were analyzed with either MetaMorph or ImageJ (National Institutes of Health) software.

FRAP

Photobleaching was performed using a FRAPPA module (Andor Technology) on the spinning-disc microscope (TE2000-E) described in the previous section. Embryos were photobleached for 3× 1-s intervals and followed for 15 min (mCherry::CPG-1) or 2 min (mCherry::CPG-2) after bleaching to monitor fluorescence recovery. For each time point, the total fluorescence was measured in equal area circles in bleached and nonbleached (control) regions of the eggshell (mCherry::CPG-1) or perivitelline space (mCherry::CPG-2). Background fluorescence was the mean fluorescence intensity of an equal-sized area in the embryo interior over the three frames immediately before photobleaching and was subtracted from the values for each time point. Fraction of initial fluorescence was calculated by dividing the total fluorescence intensity at a given time point by the mean total fluorescence intensity of the three time points immediately preceding the photobleach.

High-pressure freezing and electron microscopy

Whole worms or isolated early embryos were cryoimmobilized using a high-pressure freezer with rapid transfer system (EMPACT2; Leica). For optimal morphology, samples were freeze substituted at −90°C for 20 h in anhydrous acetone containing 1% osmium tetroxide and 0.1% uranyl acetate. The temperature was progressively raised to room temperature over 22 h in an automatic freeze substitution machine (EM AFS; Leica), and samples were embedded in thin, optically clear layers of Epon/Araldite resin. For this, samples were evenly distributed on microscope slides coated with Teflon (MS-122DF; Miller Stephenson Chemical Co.). A second coated microscope slide was placed on top, and this "sandwich" was polymerized at 60°C for 2 d (Müller-Reichert et al., 2003, 2007). The top glass slide was removed for ultramicrotomy. For immunolabeling, specimens were freeze substituted in 0.2% glutaraldehyde and 0.1% uranyl acetate and embedded in LR white (Müller-Reichert et al., 2003). A microscope slide was coated with Teflon, and a piece of a 22-mm square (Thermanox; Thermo Fisher Scientific) from which an 18-mm square had been removed from the center was glued to the slide with a Krazy Glue pen and allowed to dry for ≥1 h. Worms in pure LR white resin were placed in the 18-mm square cavity and covered with a 25-mm square piece of Aclar. The slide was placed in a container flooded with dry nitrogen gas, which was sealed and put into a 60°C oven for 1–2 d. The Aclar plastic was peeled off, and selected worms were cut out and remounted for sectioning. Thin sections (70 nm) were cut using a microtome (Ultracut UCT; Leica) and collected on Formvar-coated copper grids. Immunoelectron microscopy of CPG-1 and CPG-2 was performed using 1:500 dilutions of primary antibodies Ab153 and Ab154 and a 1:35 dilution of a secondary goat anti–rabbit antibody coupled to 10-nm colloidal gold (Kirkham et al., 2003). Immunoelectron microscopy of chitin was performed by incubating with a 1:50 dilution of maltose-binding protein–tagged chitin-binding probe (New England Biolabs, Inc.) followed by a 1:50 dilution of an antibody to maltose-binding protein (New England Biolabs, Inc.) and detection with a 1:35 dilution of goat anti–mouse antibody coupled to 10-nm colloidal gold. Sections were poststained with 2% uranyl acetate in 70% methanol followed by aqueous lead citrate and viewed in a transmission electron microscope (Tecnai 12; FEI) operated at 100 kV.

Online supplemental material

Fig. S1, which is related to Fig. 1, shows that CPG-1 and CPG-2 localize to puncta in oocytes of the proximal gonad and to the embryonic eggshell. Fig. S2, which is related to Fig. 2, shows that CPG-1 is stably incorporated into the inner layer of the eggshell, whereas CPG-2 rapidly diffuses within the perivitelline space. Video 1 shows that mCherry::CPG-1 failed to recover after photobleaching, indicating it was stably incorporated into the eggshell. Video 2 shows rapid recovery of mCherry::CPG-2 after photobleaching, indicating it was soluble in the perivitelline space. Video 3 shows that GFP::CHS-1 internalized from the plasma membrane coincident with cortical granule exocytosis at anaphase of meiosis I. Video 4 shows the formation of scallops caused by plasma membrane adhesion to the eggshell at anaphase of meiosis I in a *cpg-1/2(RNAi)* embryo. Video 5 shows rupture of an embryo through the eggshell in a *chs-1(RNAi)* embryo. Video 6 shows the permeability barrier was malleable and continually changing shape, suggesting it behaves more like a tightly drawn blanket than a rigid ECM layer. Video 7 shows prolonged cortical granule exocytosis in a *kca-1(RNAi)* embryo. Video 8 shows prolonged cortical granule exocytosis in a *pod-1(RNAi)* embryo. Table S1 lists the *C. elegans* strains used in this study. Table S2 lists the dsRNAs used in this study. Online supplemental material is available at http://www.jcb.org/cgi/content/full/jcb.201206008/DC1.

The authors thank Tony Hyman for providing us with space in his laboratory and helpful discussions during our work on the correlative light and electron microscopy experiments, Anjon Audhya for strain MSN-100, and Andy Golden, Chris Campbell, and Becky Green for thoughtful comments on the manuscript. Some nematode strains used in this work were provided by the Caenorhabditis Genetics Center, which is funded by the National Institutes of Health National Center for Research Resources.

This work was supported by funding from the Ludwig Institute for Cancer Research to K. Oegema, from the Deutsche Forschungsgemeinschaft grants MU 1423/2-1 and MU 1423/3-1 to T. Müller-Reichert, and from National Institutes of Health grant GM33063 to J.D. Esko. S.K. Olson is a San Diego Institutional Research and Academic Career Development Award Postdoctoral Fellow supported by National Institutes of Health grant GM06852.

Submitted: 4 June 2012
Accepted: 19 July 2012

References

Anya, A.O. 1976. Physiological aspects of reproduction in nematodes. *Adv. Parasitol.* 14:267–351. http://dx.doi.org/10.1016/S0065-308X(08)60516-3

Audhya, A., F. Hyndman, I.X. McLeod, A.S. Maddox, J.R. Yates III, A. Desai, and K. Oegema. 2005. A complex containing the Sm protein CAR-1 and the RNA helicase CGH-1 is required for embryonic cytokinesis in *Caenorhabditis elegans*. *J. Cell Biol.* 171:267–279. http://dx.doi.org/10.1083/jcb.200506124

Bartley, J.P., E.A. Bennett, and P.A. Darben. 1996. Structure of the ascarosides from *Ascaris suum*. *J. Nat. Prod.* 59:921–926. http://dx.doi.org/10.1021/np960236+

Bembenek, J.N., C.T. Richie, J.M. Squirrell, J.M. Campbell, K.W. Eliceiri, D. Poteryaev, A. Spang, A. Golden, and J.G. White. 2007. Cortical granule exocytosis in *C. elegans* is regulated by cell cycle components including separase. *Development*. 134:3837–3848. http://dx.doi.org/10.1242/dev.011361

Benenati, G., S. Penkov, T. Müller-Reichert, E.V. Entchev, and T.V. Kurzchalia. 2009. Two cytochrome P450s in *Caenorhabditis elegans* are essential for the organization of eggshell, correct execution of meiosis and the polarization of embryo. *Mech. Dev.* 126:382–393. http://dx.doi.org/10.1016/j.mod.2009.02.001

Bird, A.F. 1971. The Structure of Nematodes. Academic Press, New York. 318 pp.

Butcher, R.A., J.R. Ragains, W. Li, G. Ruvkun, J. Clardy, and H.Y. Mak. 2009. Biosynthesis of the *Caenorhabditis elegans* dauer pheromone. *Proc. Natl. Acad. Sci. USA*. 106:1875–1879. http://dx.doi.org/10.1073/pnas.0810338106

Carvalho, A., S.K. Olson, E. Gutierrez, K. Zhang, L.B. Noble, E. Zanin, A. Desai, A. Groisman, and K. Oegema. 2011. Acute drug treatment in the early *C. elegans* embryo. *PLoS ONE*. 6:e24656. http://dx.doi.org/10.1371/journal.pone.0024656

Cheeseman, I.M., S. Niessen, S. Anderson, F. Hyndman, J.R. Yates III, K. Oegema, and A. Desai. 2004. A conserved protein network controls assembly of the outer kinetochore and its ability to sustain tension. *Genes Dev.* 18:2255–2268. http://dx.doi.org/10.1101/gad.1234104

Chitwood, B.G. 1938. Further studies on nemic skeletoids and their significance in the chemical control of nemic pests. *Proc. Helminth. Soc. Wash.* 5:68–75.

Christenson, R.O. 1950. Nemic ova. *In* An Introduction to Nematology. B.G. Chitwood and M.G. Chitwood, editors. Monumental Printing, Baltimore, MD. 175–190.

Desai, A., S. Rybina, T. Müller-Reichert, A. Shevchenko, A. Shevchenko, A. Hyman, and K. Oegema. 2003. KNL-1 directs assembly of the microtubule-binding interface of the kinetochore in *C. elegans*. *Genes Dev.* 17:2421–2435. http://dx.doi.org/10.1101/gad.1126303

Edison, A.S. 2009. *Caenorhabditis elegans* pheromones regulate multiple complex behaviors. *Curr. Opin. Neurobiol.* 19:378–388. http://dx.doi.org/10.1016/j.conb.2009.07.007

Fairbairn, D. 1957. The biochemistry of *Ascaris*. *Exp. Parasitol.* 6:491–554. http://dx.doi.org/10.1016/0014-4894(57)90037-1

Fauré-Fremiet, E. 1913. Le cycle germinatif chez *l'Ascaris megalocephala*. *Arch. d'Anat. Micr.* 15:435–758.

Foor, W.E. 1967. Ultrastructural aspects of oocyte development and shell formation in *Ascaris lumbricoides*. *J. Parasitol.* 53:1245–1261. http://dx.doi.org/10.2307/3276689

Fouquey, C., J. Polonsky, and E. Lederer. 1957. Chemical structure of ascarylic alcohol isolated from *Parascaris equorum*. [In French.] *Bull. Soc. Chim. Biol. (Paris)*. 39:101–132.

Green, R.A., H.-L. Kao, A. Audhya, S. Arur, J.R. Mayers, H.N. Fridolfsson, M. Schulman, S. Schloissnig, S. Niessen, K. Laband, et al. 2011. A high-resolution *C. elegans* essential gene network based on phenotypic profiling of a complex tissue. *Cell*. 145:470–482. http://dx.doi.org/10.1016/j.cell.2011.03.037

Harlow, E., and D. Lane. 1988. Antibodies: A Laboratory Manual. Cold Spring Harbor Press, Cold Spring Harbor, NY. 726 pp.

Jezyk, P.F., and D. Fairbairn. 1967. Ascarosides and ascaroside esters in *Ascaris lumbricoides* (Nematoda). *Comp. Biochem. Physiol.* 23:691–705. http://dx.doi.org/10.1016/0010-406X(67)90334-9

Johnston, W.L., A. Krizus, and J.W. Dennis. 2006. The eggshell is required for meiotic fidelity, polar-body extrusion and polarization of the *C. elegans* embryo. *BMC Biol.* 4:35. http://dx.doi.org/10.1186/1741-7007-4-35

Johnston, W.L., A. Krizus, and J.W. Dennis. 2010. Eggshell chitin and chitin-interacting proteins prevent polyspermy in *C. elegans*. *Curr. Biol.* 20:1932–1937. http://dx.doi.org/10.1016/j.cub.2010.09.059

Kirkham, M., T. Müller-Reichert, K. Oegema, S. Grill, and A.A. Hyman. 2003. SAS-4 is a *C. elegans* centriolar protein that controls centrosome size. *Cell*. 112:575–587. http://dx.doi.org/10.1016/S0092-8674(03)00117-X

Krakow, N.P. 1892. Ueber verschiedenartige Chitine. *Zeitschr. Biol*. 29: 177–198.

Lee, J.-Y., and B. Goldstein. 2003. Mechanisms of cell positioning during *C. elegans* gastrulation. *Development*. 130:307–320. http://dx.doi.org/10.1242/dev.00211

Lehane, M.J. 1997. Peritrophic matrix structure and function. *Annu. Rev. Entomol.* 42:525–550. http://dx.doi.org/10.1146/annurev.ento.42.1.525

Liu, J., S. Vasudevan, and E.T. Kipreos. 2004. CUL-2 and ZYG-11 promote meiotic anaphase II and the proper placement of the anterior-posterior axis in *C. elegans*. *Development*. 131:3513–3525. http://dx.doi.org/10.1242/dev.01245

Mansfield, L.S., H.R. Gamble, and R.H. Fetterer. 1992. Characterization of the eggshell of *Haemonchus contortus*—I. Structural components. *Comp. Biochem. Physiol. B*. 103:681–686. http://dx.doi.org/10.1016/0305-0491(92)90390-D

Maruyama, R., N.V. Velarde, R. Klancer, S. Gordon, P. Kadandale, J.M. Parry, J.S. Hang, J. Rubin, A. Stewart-Michaelis, P. Schweinsberg, et al. 2007. EGG-3 regulates cell-surface and cortex rearrangements during egg activation in *Caenorhabditis elegans*. *Curr. Biol.* 17:1555–1560. http://dx.doi.org/10.1016/j.cub.2007.08.011

McNally, K., A. Audhya, K. Oegema, and F.J. McNally. 2006. Katanin controls mitotic and meiotic spindle length. *J. Cell Biol.* 175:881–891. http://dx.doi.org/10.1083/jcb.200608117

Monen, J., P.S. Maddox, F. Hyndman, K. Oegema, and A. Desai. 2005. Differential role of CENP-A in the segregation of holocentric *C. elegans* chromosomes during meiosis and mitosis. *Nat. Cell Biol.* 7:1248–1255. http://dx.doi.org/10.1038/ncb1331

Müller-Reichert, T., H. Hohenberg, E.T. O'Toole, and K. McDonald. 2003. Cryoimmobilization and three-dimensional visualization of *C. elegans* ultrastructure. *J. Microsc.* 212:71–80. http://dx.doi.org/10.1046/j.1365-2818.2003.01250.x

Müller-Reichert, T., M. Srayko, A. Hyman, E.T. O'Toole, and K. McDonald. 2007. Correlative light and electron microscopy of early *Caenorhabditis elegans* embryos in mitosis. *Methods Cell Biol.* 79:101–119. http://dx.doi.org/10.1016/S0091-679X(06)79004-5

Natsuka, S., M. Kawaguchi, Y. Wada, A. Ichikawa, K. Ikura, and S. Hase. 2005. Characterization of wheat germ agglutinin ligand on soluble glycoproteins in *Caenorhabditis elegans*. *J. Biochem.* 138:209–213. http://dx.doi.org/10.1093/jb/mvi117

Oegema, K., A. Desai, S. Rybina, M. Kirkham, and A.A. Hyman. 2001. Functional analysis of kinetochore assembly in *Caenorhabditis elegans*. *J. Cell Biol.* 153:1209–1226. http://dx.doi.org/10.1083/jcb.153.6.1209

Olson, S.K., J.R. Bishop, J.R. Yates, K. Oegema, and J.D. Esko. 2006. Identification of novel chondroitin proteoglycans in *Caenorhabditis elegans*: embryonic cell division depends on CPG-1 and CPG-2. *J. Cell Biol.* 173:985–994. http://dx.doi.org/10.1083/jcb.200603003

Pelletier, L., E. O'Toole, A. Schwager, A.A. Hyman, and T. Müller-Reichert. 2006. Centriole assembly in *Caenorhabditis elegans*. *Nature*. 444:619–623. http://dx.doi.org/10.1038/nature05318

Praitis, V., E. Casey, D. Collar, and J. Austin. 2001. Creation of low-copy integrated transgenic lines in *Caenorhabditis elegans*. *Genetics*. 157:1217–1226.

Rappleye, C.A., A.R. Paredez, C.W. Smith, K.L. McDonald, and R.V. Aroian. 1999. The coronin-like protein POD-1 is required for anterior-posterior axis formation and cellular architecture in the nematode *Caenorhabditis elegans*. *Genes Dev.* 13:2838–2851. http://dx.doi.org/10.1101/gad.13.21.2838

Rappleye, C.A., A. Tagawa, N. Le Bot, J. Ahringer, and R.V. Aroian. 2003. Involvement of fatty acid pathways and cortical interaction of the pronuclear complex in *Caenorhabditis elegans* embryonic polarity. *BMC Dev. Biol.* 3:8. http://dx.doi.org/10.1186/1471-213X-3-8

Rogers, R.A. 1956. A study of eggs of *Ascaris lumbricoides* var. suum with the electron microscope. *J. Parasitol.* 42:97–108. http://dx.doi.org/10.2307/3274720

Sato, K., M. Sato, A. Audhya, K. Oegema, P. Schweinsberg, and B.D. Grant. 2006. Dynamic regulation of caveolin-1 trafficking in the germ line and embryo of *Caenorhabditis elegans*. *Mol. Biol. Cell*. 17:3085–3094. http://dx.doi.org/10.1091/mbc.E06-03-0211

Sato, M., B.D. Grant, A. Harada, and K. Sato. 2008. Rab11 is required for synchronous secretion of chondroitin proteoglycans after fertilization in *Caenorhabditis elegans*. *J. Cell Sci.* 121:3177–3186. http://dx.doi.org/10.1242/jcs.034678

Schierenberg, E., and B. Junkersdorf. 1992. The role of eggshell and underlying vitelline membrane for normal pattern formation in the early *C. elegans* embryo. *Roux's Arch. Dev. Biol.* 202:10–16. http://dx.doi.org/10.1007/BF00364592

Schuel, H., J.W. Kelly, E.R. Berger, and W.L. Wilson. 1974. Sulfated acid mucopolysaccharides in the cortical granules of eggs. Effects of quaternary ammonium salts on fertilization. *Exp. Cell Res.* 88:24–30. http://dx.doi.org/10.1016/0014-4827(74)90613-2

Sonneville, R., and P. Gönczy. 2004. Zyg-11 and cul-2 regulate progression through meiosis II and polarity establishment in *C. elegans*. *Development*. 131:3527–3543. http://dx.doi.org/10.1242/dev.01244

Stitzel, M.L., K.C.-C. Cheng, and G. Seydoux. 2007. Regulation of MBK-2/Dyrk kinase by dynamic cortical anchoring during the oocyte-to-zygote transition. *Curr. Biol.* 17:1545–1554. http://dx.doi.org/10.1016/j.cub.2007.08.049

Tagawa, A., C.A. Rappleye, and R.V. Aroian. 2001. Pod-2, along with pod-1, defines a new class of genes required for polarity in the early *Caenorhabditis elegans* embryo. *Dev. Biol.* 233:412–424. http://dx.doi.org/10.1006/dbio.2001.0234

Tarr, G.E., and D. Fairbairn. 1973. Ascarosides of the ovaries and eggs of *Ascaris lumbricoides* (Nematoda). *Lipids*. 8:7–16. http://dx.doi.org/10.1007/BF02533232

Thibodeaux, C.J., C.E. Melançon, and H.-W. Liu. 2007. Unusual sugar biosynthesis and natural product glycodiversification. *Nature*. 446:1008–1016. http://dx.doi.org/10.1038/nature05814

Timm, R.W. 1950. Chemical composition of the vitelline membrane of *Ascaris lumbricoides* var. *suis*. *Science*. 112:167–168. http://dx.doi.org/10.1126/science.112.2902.167

Wharton, D. 1980. Nematode egg-shells. *Parasitology*. 81:447–463. http://dx.doi.org/10.1017/S003118200005616X

Wong, J.L., and G.M. Wessel. 2006. Defending the zygote: search for the ancestral animal block to polyspermy. *Curr. Top. Dev. Biol.* 72:1–151. http://dx.doi.org/10.1016/S0070-2153(05)72001-9

Wong, J.L., and G.M. Wessel. 2008. Renovation of the egg extracellular matrix at fertilization. *Int. J. Dev. Biol.* 52:545–550. http://dx.doi.org/10.1387/ijdb.072557jw

Zagoriy, V., V. Matyash, and T. Kurzchalia. 2010. Long-chain O-ascarosyl-alkanediols are constitutive components of *Caenorhabditis elegans* but do not induce dauer larva formation. *Chem. Biodivers.* 7:2016–2022. http://dx.doi.org/10.1002/cbdv.201000012

Zhang, Y., J.M. Foster, L.S. Nelson, D. Ma, and C.K.S. Carlow. 2005. The chitin synthase genes chs-1 and chs-2 are essential for *C. elegans* development and responsible for chitin deposition in the eggshell and pharynx, respectively. *Dev. Biol.* 285:330–339. http://dx.doi.org/10.1016/j.ydbio.2005.06.037